Author Manuscript

Author Manuscript

Author Manuscript

Author Manuscript

HHS Public Access

Author manuscript

Cell Metab. Author manuscript; available in PMC 2021 June 02.

Published in final edited form as:

Cell Metab. 2020 June 02; 31(6): 1091–1106.e6. doi:10.1016/j.cmet.2020.04.017.

Pseudomonas aeruginosa utilizes host-derived itaconate to redirect its metabolism to promote biofilm formation

Sebastián A. Riquelme[1], **Kalle Liimatta**[1], **Tania Wong Fok Lung**[1], **Blanche Fields**[1], **Danielle Ahn**[1], **David Chen**[1], **Carmen Lozano**[2], **Yolanda Saénz**[2], **Anne-Catrin Uhlemann**[3], **Barbara C. Kahl**[4], **Clemente J. Britto**[5], **Emily DiMango**[3], **Alice Prince**[1,*,#]

[1]Department of Pediatrics, Columbia University, New York, NY 10032, USA;

[2]Area de Microbiología Molecular, Centro de Investigación Biomédica de la Rioja (CIBIR), Microbiología Molecular, Logroño, LG 26006, Spain;

[3]Department of Medicine, Columbia University Medical Center, New York, NY 10032, USA;

[4]Institute of Medical Microbiology, University Hospital Münster, Münster 48149, Germany;

[5]Section of Pulmonary, Critical Care, and Sleep Medicine, Yale University School of Medicine, New Haven, CT 06520, USA.

Abstract

The bacterium *Pseudomonas aeruginosa* is especially pathogenic, often being associated with intractable pneumonia and high mortality. How *P. aeruginosa* avoids immune clearance and persists in the inflamed human airway remains poorly understood. In this study, we show that *P. aeruginosa* can exploit the host immune response to maintain infection. Notably, unlike other opportunistic bacteria, we found that *P. aeruginosa* alters its metabolic and immunostimulatory properties in response to itaconate, an abundant host-derived immunometabolite in the infected lung. Itaconate induces bacterial membrane stress, resulting in downregulation of lipopolysaccharides (LPS) and upregulation of extracellular polysaccharides (EPS). These itaconate-adapted *P. aeruginosa* accumulate *lptD* mutations, which favor itaconate assimilation and biofilm formation. EPS, in turn, induces itaconate production by myeloid cells, both in the airway and systemically, skewing the host immune response to one permissive of chronic infection. Thus, the metabolic versatility of *P. aeruginosa* needs to be taken into account when designing therapies.

*Correspondence can be sent to Alice Prince, senior author of this manuscript (asp7@columbia.edu.).

#Alice Prince is the lead contact for this manuscript: Department of Pediatrics, Columbia University, New York, NY 10032, USA. Phone: +1-212-305-4193;

Author Contributions:

S.A.R. proposed the central hypothesis, conducted experiments and wrote the manuscript. K.L., T.W., C.L., D.C., D.A. and B.F. conducted experiments and wrote the manuscript. B.K. and A.C.U. provided with clinical isolates. E.D. provided with human samples. C.J.B. provided with sputum samples. A.P. proposed central hypothesis and wrote the manuscript.

Publisher's Disclaimer: This is a PDF file of an unedited manuscript that has been accepted for publication. As a service to our customers we are providing this early version of the manuscript. The manuscript will undergo copyediting, typesetting, and review of the resulting proof before it is published in its final form. Please note that during the production process errors may be discovered which could affect the content, and all legal disclaimers that apply to the journal pertain.

Supplemental Information: This study counts with 7 Supplemental Figures that can be found in the online version of this manuscript.

Competing Interest: Authors declare that no conflicts of interest exist.

Author Manuscript Author Manuscript Author Manuscript Author Manuscript

Graphical Abstract

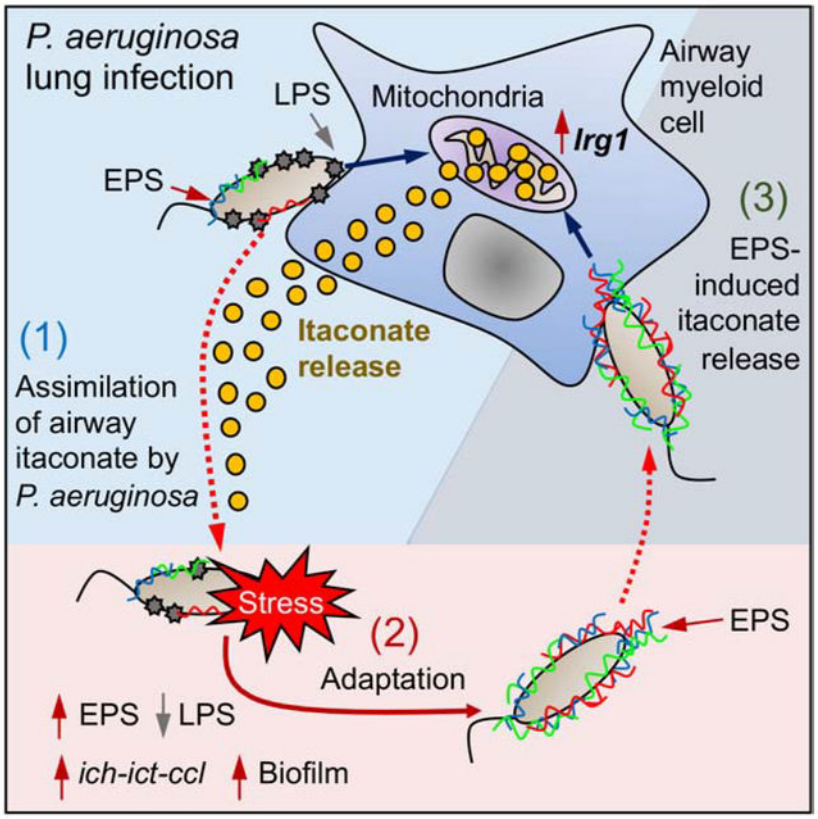

eTOC blurb

The ability of *Pseudomonas aeruginosa* to chronically infect the lungs of immunocompetent individuals suggests these organisms might utilize aspects of the host defense system to their advantage. Riquelme *et al* demonstrate how *P. aeruginosa* exploits itaconate, a major mitochondrial metabolite produced by immune cells to thwart effective immune clearance, to promote biofilm formation.

Introduction

Metabolic activation of myeloid cells is a key component of innate immune clearance of airway infection. Upon encountering lipopolysaccharide (LPS), the major immunostimulatory component of Gram-negative pathogens, macrophages and monocytes increase aerobic glycolysis, generate and oxidize succinate resulting in the synthesis of the potent anti-bacterial cytokine IL-1β (Mills et al., 2016; Mills et al., 2017; Tannahill et al., 2013). The inflammation and release of oxidants damages both bacteria and local tissue. In response to oxidant stress, myeloid cells upregulate immune-response gene 1 (*Irg1*) expression (Mills et al., 2018), which synthetizes the carboxylate metabolite itaconate that suppresses both glycolysis (Qin et al., 2019) and succinate catabolism (Lampropoulou et al., 2016). Itaconate serves to recover tissue homeostasis by deactivating effector immune cells. Itaconate is one of the most abundant metabolites produced by myeloid cells in response to

Author Manuscript Author Manuscript Author Manuscript Author Manuscript

infection and a major activator of the host anti-oxidant response (Lampropoulou et al., 2016; Mills et al., 2018). However, accumulation of the immunometabolites itaconate and succinate may have additional consequences, by providing substrates and imposing selective pressure on infecting organisms with sufficient genomic and metabolic plasticity to adapt (Riquelme et al., 2019; Sasikaran et al., 2014).

Bacterial pneumonia remains a global problem, actually increasing in prevalence in some populations as a complication of increased longevity and expanded intensive-care unit (ICU) and health-care associated infections (Wunderink and Waterer, 2017). While the emergence of antibiotic resistance complicates treatment, not all antibiotic-resistant pathogens have emerged as global threats to health. *Pseudomonas aeruginosa* is a Gram-negative pathogen associated with high morbidity and mortality even in hosts with normal immune function, such as in individuals with health-care associated pneumonia (Fernandez-Barat et al., 2017; Wunderink and Waterer, 2017), chronic-obstructive pulmonary disease (COPD) (Garcia-Nunez et al., 2017) or cystic fibrosis (CF) (Deretic et al., 1995; Elborn, 2016; Winstanley et al., 2016). The bacterium has achieved a CDC and WHO designation as one of the most feared pathogens worldwide (Kubes and Fridkin, 2019; World-Health-Organization, 2017). Despite inducing a robust LPS-mediated acute inflammatory response, *P. aeruginosa* persists within the airways by forming intractable biofilms. Among many factors, the tremendous metabolic flexibility harbored in the large genome of *P. aeruginosa* enables this pathogen to readily adapt to conditions in the airway and especially to the immune metabolic program that is activated in response to infection.

The extraordinary success of antibiotic-resistant pathogens such as *P. aeruginosa* depends on their capacity to actively adapt to and efficiently consume available local nutrients, often in the presence of extensive myeloid cell recruitment. Activated monocytes and macrophages release substantial amounts of both succinate, a known *P. aeruginosa* substrate (Collier et al., 1996; Gorke and Stulke, 2008; Riquelme et al., 2019; Rojo, 2010), as well as itaconate, which it and other highly pathogenic airway bacteria, such as *M. tuberculosis*, can potentially metabolize *in vivo* (Wang et al., 2019). In this study, based upon human clinical isolates of *P. aeruginosa*, and in contrast to the standard laboratory strains, we demonstrate that itaconate selects metabolically-adapted *P. aeruginosa* strains with increased resistance to oxidant stress generated by altered bacterial metabolic activity and substantially increased synthesis of extracellular polysaccharides (EPS), as well as providing a mechanism outlining this process. Namely, we found that mature LPS, expected to be the major surface immunostimulatory component of *P. aeruginosa*, is replaced by EPS in the presence of itaconate. EPS not only protect the bacteria from oxidants, they trigger myeloid cell metabolic reprogramming, both locally and in circulating monocytes, to induce even greater itaconate release. This host and pathogen metabolic adaptation generates a self-perpetuating bacterial community and provides a steady supply of antibiotic-resistant pathogens.

Author Manuscript Author Manuscript Author Manuscript Author Manuscript

RESULTS AND DISCUSSION

Clinical isolates of *P. aeruginosa* undergo an adaptive change in expression of LPS and EPS

P. aeruginosa exhibits a dynamic metabolic network that coordinates energy production and the generation of multiple macromolecules, such as LPS and EPS (FIGURE 1A, blue and red boxes). While TCA cycle activity is mostly associated with ATP generation (FIGURE 1A, yellow circle), glucose metabolism is bidirectional, and can be reprogramed to shunt carbohydrates either into synthesis of LPS, protective EPS (gluconeogenesis, FIGURE 1A red arrows) or to produce energy (Entner-Duodoroff and Embden-Meyerhof Pathways, FIGURE 1A orange and green boxes, respectively). EPS production is favored in response to bacterial outer-membrane stress, which is mainly triggered by pro-oxidants and bactericidal components of host immunity. Gluconeogenesis and EPS synthesis can be supported by the glyoxylate shunt, an abbreviated TCA cycle that under stress is primed by acetyl-coA (FIGURE 1A, purple box). Itaconate is also a source of acetyl-coA (FIGURE 1A, gray box), suggesting this immunometabolite might fuel EPS synthesis. We postulated that virtually all isolates of *P. aeruginosa* from chronically infected sites, such as wounds or the airways, must undergo metabolic changes to cope with the oxidants imposed by the recruited immune response. Thus, we analyzed published transcriptional data from *P. aeruginosa* isolates derived from several sites of infection in immunocompetent hosts to assess *in vivo*-acquired metabolic changes associated with outer-membrane stress; namely, changes in LPS and EPS synthesis (FIGURE 1B). These isolates included strains from sputum of individuals with CF and soft-tissue samples from subjects with chronic and burn wound infections (Cornforth et al., 2018). We compared these expression changes with those of *P. aeruginosa* isolates obtained from 40-h acute burn and 4-day non-diabetic chronic wound infections from mice (Turner et al., 2014). The most consistently upregulated genes were those involved in activating the EPS alginate operon, such as the outer membrane stress-related sigma factor *algT* (also known as *algU*) and its co-expressed regulator *mucA* (FIGURE 1B, red group). *AlgW*, which encodes a *mucA* protease, was partially downregulated. *AlgA* and *algR* were upregulated, as was *algD*, loci that are under the control of *algT* during surface perturbations. While alginate over-production is typically associated with CF-related strains of *P. aeruginosa* (Deretic et al., 1995), the genes regulating its expression are upregulated in many other clinical settings. Less consistent were the effects on the expression of the EPS genes *pelA* (Pel) and *pslA* (Psl), which varied depending on the source of the organism analyzed (FIGURE 1B, red group). In contrast, in most of the studies there was decreased expression of genes involved in endotoxin and O-antigen assembly, including many multi-operon genes, such as *wzy*, *wbpA*, *wbpG*, *wbpY* (FIGURE 1B, blue group). LptD, the outer membrane protein that translocates LPS to the bacterial surface was also decreased (FIGURE 1B, blue group) (Balibar and Grabowicz, 2016; Botos et al., 2016), resulting in accumulation of LPS in the periplasmic space. These findings suggest that, once in the host, *P. aeruginosa* from various sites decreases LPS synthesis and its trafficking, a response associated with outer-membrane stress, while also increasing *algT* expression, which would increase production of EPS (Lima et al., 2013).

Author Manuscript Author Manuscript Author Manuscript Author Manuscript

P. aeruginosa consumes mitochondrial metabolites

These changes in the EPS and LPS pathways in *P. aeruginosa* isolates are likely induced by inflammatory cells at sites of infection and the presence of myeloid metabolites, such as succinate and itaconate (Lampropoulou et al., 2016; Tannahill et al., 2013). We used clinical isolates from individuals with CF to first establish whether *P. aeruginosa* induces accumulation of itaconate, succinate and glucose in the airway as compared to the laboratory strain WT PAO1 (referred to as simply PAO1 hereafter). Using a mouse model of pneumonia, we found host-adapted isolates induced significantly more itaconate secretion into the bronchoalveolar lavage (BAL), as compared with responses to PAO1, the latter of, in contrast, induced greater secretion of succinate and glucose into the BAL (FIGURE 1C). Thus, *P. aeruginosa* induces the production of immunometabolites, but the relative amounts of these correlates with the extent of the balance of bacterial EPS-to-LPS-related gene expression.

P. aeruginosa can use a variety of carbon sources depending on growth conditions; namely, aerobic or anaerobic conditions and exponential versus stationary phase growth (Arai, 2011). To evaluate the preferences of *P. aeruginosa* isolates we monitored growth in succinate, glucose or itaconate. As host-adapted strains from different subjects with CF exhibited variable growth rates, we focused on their growth in itaconate and glucose with respect to succinate, the last of which is expected to be the preferred *P. aeruginosa* carbon source (Collier et al., 1996; Gorke and Stulke, 2008; O'Toole et al., 2000; Rojo, 2010). We found that host-adapted strains reached stationary growth phase faster than PAO1 (Figure S1A) and produced more biomass in itaconate or glucose than succinate at later time points (FIGURE 1D). In this same time-frame *P. aeruginosa* strains isolated from acute infections in the ICU, as well as the laboratory control strains PAO1 and PA14, generally grew exponentially (Figure S1A) and preferred succinate or grew equally well on all three substrates (FIGURE 1D). These data indicate that airway-adapted *P. aeruginosa* strains, which gain EPS production over LPS synthesis, display a differential dynamic growth pattern from laboratory strains with the former exhibiting a specific preference for itaconate and glucose over succinate.

Itaconate promotes expression of anti-membrane stress EPS and suppresses LPS assembly

The preferential consumption of itaconate and glucose as primary carbon sources by the apparently LPS-deficient host-adapted *P. aeruginosa* isolates and their increased expression of *algD*, *pelA* and *pslA*, suggested that itaconate promotes EPS synthesis. Itaconate belongs to the group of electrophiles (Bambouskova et al., 2018), known to trigger the *P. aeruginosa* stress defense response (Juarez et al., 2017; Wongsaroj et al., 2018). We found that when added to glucose (1:1), itaconate induced substantial variation in *P. aeruginosa* size (FIGURE S1B) and surface granularity (FIGURE S1C), changes expected in response to superficial damage and membrane distress. By using the *bac*light $DiOC_2(3)$ membrane potential dye, we studied changes in bacterial surface homeostasis. This dye accumulates inside bacteria and emits green fluorescence in direct proportion with size. Under active oxidative phosphorylation (OXPHOS), this dye also emits red fluorescence, as it senses the transport of protons from the cytoplasm and their accumulation at the periplasmic space.

Author Manuscript Author Manuscript Author Manuscript Author Manuscript

The red-to-green color ratio can be used to track changes in bacterial membrane potential. We observed that despite accumulating more intrabacterial green dye due to their increased size (FIGURE S1D), itaconate-treated *P. aeruginosa* did not exhibit a proportional increase in red fluorescence (FIGURE S1E), which was interpreted as a reduced membrane potential (FIGURE 1E). This finding suggested that itaconate reduced OXPHOS in *P. aeruginosa*. However, these organisms produced the same amount of OXPHOS-derived anion superoxide ($O_2{*}^-$) with or without itaconate (FIGURE S1F), suggesting this immunometabolite also induces proton leakage from the periplasm into the extracellular space through a permissive outer membrane. This membrane potential diffusion, irregular surface granularity and the partial production of LPS core but not O-antigen in *P. aeruginosa* PAO1 (FIGURE 1F) is consistent with the selection of variants exhibiting membrane perturbation and rough LPS, as often seen in CF (Evans et al., 1994). Outer membrane stress and lack of O-antigen production was consistent with downregulation of genes involved in LPS biosynthesis and its trafficking by itaconate, including *wbpA*, *wbpG*, *wbpY*, and *lptD* (FIGURE 1G). In response to this pressure, itaconate-treated PAO1 induced overexpression of the membrane anti-stress *algT* locus, which corresponded with increased levels of *algA*, *algD*, *algR* and *algQ* (FIGURE 1G). *MucA*, which is co-transcribed with the EPS alginate operon, was also upregulated along with *pelA* and *pslA* expression (FIGURE 1G), confirming the positive role of itaconate inducing the protective EPS machinery instead of LPS synthesis due to membrane deregulation.

P. aeruginosa lacking surface LPS activates macrophage metabolism

Surface-exposed LPS is arguably the major immunostimulatory component of *P. aeruginosa*, inducing TLR4 signaling in macrophages that activates pro-inflammatory gene expression. Cytokine production is supported by profound metabolic changes in macrophages such as succinate production, its oxidation by mitochondria, HIF-1α induction and increased glycolysis (Mills et al., 2016; Mills et al., 2017; Tannahill et al., 2013). Rapid alterations in LPS biosynthesis or its surface display, such as those due to lack of *lptD* function in host-adapted *P. aeruginosa*, are expected to have major consequences on bacterial membrane-stress responses (Lima et al., 2013) and immune cell activation (Mills et al., 2016). We predicted that mutants lacking surface-exposed LPS would experience stress, outer membrane permeability and lose immunogenicity. We used a Δ*lptD*4213 PAO1 mutant, which harbors a 23 amino acid depletion (Figure S2A) in an extracellular loop that produces a truncated LptD protein (Balibar and Grabowicz, 2016; Lee et al., 2016) unable to traffic LPS to the bacterial surface, to evaluate the effects of periplasmic LPS accumulation on *P. aeruginosa* immunogenicity. These strains display external barrier destabilization (Balibar and Grabowicz, 2016), and antibodies that bind LPS-related sugars penetrate their outer membranes, allowing for the detection of increased levels of endotoxin components accumulated in the periplasmic region (Figure S2B). Using mouse bone marrow-derived macrophages (BMDMs) we observed that the Δ*lptD*4213 PAO1 mutant induced even higher extracellular acidification rates (ECAR, lactate production: glycolysis) than did the WT control (FIGURE 2A), suggesting that these strains were fully metabolo-stimulatory. Although to a lesser extent, mitochondrial ROS ($O_2{*}^-$) production in BMDMs was also induced by these mutant organisms (FIGURE 2B), and oxygen consumption rates (OCRs) were increased by both WT and Δ*lptD*4213 strains with respect to PBS-treated cells and

Author Manuscript Author Manuscript Author Manuscript Author Manuscript

only differed before glucose addition (FIGURE 2C). These data suggest that in metabolically active *P. aeruginosa* LPS surface expression is not necessarily the major inducer of macrophage metabolic changes.

We next tested the immunostimulatory consequences of the Δ*lptD*4213 strain as compared with PAO1 in a mouse model of pneumonia. Both strains induced similar amounts of chemoattractants, such as Rantes, Eotaxin, CCL12, CCL17, CCL19, CCL20, CCL21, CCL22, MCP-1, GCS-F, GM-CSF and VGEF (FIGURE S2C). We found equivalent numbers of alveolar macrophages (FIGURE S2D–E) and $Ly6C^{+/-}$ $Ly6G^{+}$ neutrophils and $Ly6C^{High}Ly6G^{-}$ monocytes in the BAL (FIGURE S2F–G) and lungs (FIGURE S2H). Thus, lack of surface LPS did not inhibit signaling to attract phagocytes. However, due to lack of TLR4 signaling mice infected with the LPS-mutants had significantly less IL-1β, IL-6 and TNFα secretion into the airways, as compared with PAO1 (FIGURE 2D), indicating that *lptD* dysfunction in *P. aeruginosa* results in the activation of thwarted airway inflammatory response, as we predicted. Nevertheless, this qualitatively different response triggered by LPS-mutant *P. aeruginosa* conserved the metabolic changes associated with macrophage activation.

LptD-mutant *P. aeruginosa* stimulates itaconate production for bacterial metabolism

The induction of oxidative metabolism in macrophages by Δ*lptD*4213 PAO1 implied that these mutants could also trigger the mitochondrial anti-oxidant program. In response to oxidative metabolism, mitochondria upregulate *Irg1* expression, which produces the anti-oxidant intermediate itaconate (Lampropoulou et al., 2016; Mills et al., 2018). We observed that *Irg1* was required to suppress macrophages OCR (FIGURE 2E) but not glycolysis (FIGURE 2F) during Δ*lptD*4213 infection, and in a mouse model of pneumonia these Δ*lptD*4213 mutants induced greater amounts of itaconate accumulation in the BAL than the PAO1 control (FIGURE 2G). These findings suggest that despite lacking surface LPS, these *lptD P. aeruginosa* mutants induce *Irg1* activity and itaconate production to suppress pro-oxidant mitochondrial activities.

The release of itaconate subjects *P. aeruginosa* to a major selective pressure as itaconate is bactericidal (Naujoks et al., 2016; Rittenhouse and McFadden, 1974), though the bacterium can consume itaconate by upregulating the *ict-ich-ccl* locus (Sasikaran et al., 2014). We found that both PAO1 and Δ*lptD*4213 responded to itaconate by upregulating these genes (FIGURE S2I), and both strains grew in itaconate to a similar extent during the exponential (no differences) and stationary growth phase (24% difference) (FIGURE 2H and FIGURE S2J). However, lack of *lptD* function caused a higher reduction in PAO1 growth in succinate (56%) and glucose (34%) at both early and late time points (FIGURE 2H and FIGURE S2J), suggesting that LPS deregulations are associated with preservation of itaconate as a major carbon source. Moreover, growth in itaconate resulted in increased production of biofilm (FIGURE 2I), more so than in succinate (FIGURE 2J), which was expected to be the preferred carbon source for PAO1 (Collier et al., 1996; Gorke and Stulke, 2008; Rojo, 2010). This preference for itaconate by mutant PAO1 was manifested *in vivo*. Pulmonary infection with this Δ*lptD*4213 strain was significantly greater in WT mice compared to mice unable to produce itaconate (i.e., *Irg1*$^{-/-}$ mice) as we saw a 95% decrease in the level of bacterial

Author Manuscript Author Manuscript Author Manuscript Author Manuscript

colony forming units (CFUs) with infection of the knockout mice vs. the WT mice (FIGURE 2K). However, the Δ*lptD*4213 strain elicited similar numbers of immune cells into the airway of WT and *Irg1*$^{-/-}$ mice (FIGURE S2K–L), suggesting the mutation did not interfere with initial immune recognition of the pathogen. In total these data suggest that lack of *lptD* function and thus reduced accumulation of LPS in the bacterial periplasm tunes both bacterial and immune cell activities as a consequence of itaconate metabolism.

EPS alginate activates macrophage immunometabolism

We were surprised to find that *P. aeruginosa* with substantial defects in LPS display, nonetheless, activates glycolysis and mitochondrial respiration in myeloid cells (FIGURE 2A–C and FIGURE 2G). Given that the Δ*lptD*4213 strain upregulated the cascade of pro-EPS genes, including *algT* and *algD*, as compared to PAO1 (FIGURE 2L), we postulated that EPS, especially alginate, might induce changes in macrophage metabolism. Though typically associated with CF strains, alginate production is a feature, to varying degrees, of *P. aeruginosa* infections in acute and chronic infections (Bragonzi et al., 2005; Franklin et al., 2011; Hentzer et al., 2001), as we observed (FIGURE 1B). The immunometabolic effects of alginate on macrophages were assessed by measuring changes in ECAR and OCR, and we found that soluble alginate increased ECAR but not mitochondrial respiration in treated BMDMs (FIGURE 3A–B), similar to what was observed with LPS. We demonstrated these alginate effects were specific, as neither polyethylene glycol (PEG) nor N-acetyl glucosamine, a major bacterial cell wall component (Dhar et al., 2018), induced ECAR or increased OCR in BMDMs (FIGURE S3A). We further found that alginate increased the mitochondrial membrane potential (ΔΨ) without augmenting ROS production by macrophages (FIGURE 3C–D), indicating that this EPS alone causes mitochondrial deregulation probably due to augmented glycolysis as seen with LPS (Mills et al., 2016).

AlgD expression modulates macrophage metabolism and immunotoxicity of *P. aeruginosa*

To confirm the effects of alginate expressed by living organisms on host metabolic activity, we used an Δ*algD* mutant in the PAO1 background, which cannot synthetize alginate. This Δ*algD* and its WT PAO1 control generate the same amount of LPS (Goldberg et al., 1995). We observed that the Δ*algD* strain was apparently toxic to mammalian macrophages in our attempts to monitor induced ECAR (FIGURE 3E). Macrophages treated with the Δ*algD* PAO1 had higher initial OCR than those exposed to PAO1, which rapidly declined after glucose administration (FIGURE 3F). Mitochondrial dysfunction was confirmed after observing that Δ*algD* readily reduced the ΔΨ independent of the amounts of O_2^{*-} induced (FIGURE 3G–H).

These results suggest that bacterial alginate metabolism might protect macrophages from both a glucose- and ΔΨ-dependent cell death pathway. We observed that lack of *algD* not only reduced *algT*, *algR* and *mucA* expression in PAO1, it also induced synthesis of translocons *pcrV-popD* and e*xoT-exoS* toxins, both components of the type three secretion system (T3SS) (FIGURE S3B–C). The *P. aeruginosa* T3SS is known for inducing mitochondrial damage and a highly pro-inflammatory type of cell death called pyroptosis, which is associated with IL-1β production (Evavold et al., 2018; Faure et al., 2014; Jabir et al., 2015). To test this hypothesis *in vivo*, we infected mice intranasally with either Δ*algD* or

Author Manuscript Author Manuscript Author Manuscript Author Manuscript

WT PAO1. Mice infected with the Δ*algD* harbored greater numbers of dead alveolar macrophages in the BAL than those infected with the control PAO1 (FIGURE 4A and FIGURE S3D). Cell death was also reflected in reduced numbers of viable alveolar macrophages, Ly6C^{High}Ly6G^{-} monocytes and neutrophils in the BAL of Δ*algD*-infected mice (FIGURE 4B and FIGURE S3E–F).

We also found that Δ*algD*-infected animals secreted significantly ($P < 0.0001$) more IL-1β, but not more IL-6 or TNFα than controls (FIGURE 4C), consistent with the hypothesis that alginate suppresses the induction of pyroptosis in immune cells. We confirmed that alginate synthesis promoted more itaconate accumulation in the BAL (FIGURE 4D). In addition, this itaconate production correlated with reduced IL-1β release specifically (i.e., no change in IL-6 or TNFα) compared to that seen in the *Irg1* knockout mouse (FIGURE 4E). These findings suggest that in the presence of LPS, alginate production by *P. aeruginosa* suppresses T3SS activity, IL-1β production and pyroptotic cell death, facilitating accumulation of itaconate-producing host immune cells.

Itaconate suppresses glucose utilization by *P. aeruginosa* and promotes monocyte accumulation

We next addressed how *P. aeruginosa* supports increased EPS production in the setting of itaconate utilization as a major substrate. In *P. aeruginosa*, glucose is mainly consumed by the Entner-Duodoroff pathway, with *zwf* (glucose-6-phosphate dehydrogenase: G6PDH) as the rate limiting step (Kim et al., 2008; Ma et al., 1998; Maleki et al., 2015) (FIGURE 1A, orange box). We analyzed a mouse and two human cohorts of *P. aeruginosa* isolates (Figure 1B) which indicated that in the acute and chronic setting of infections *zwf* and several downstream pro-glycolytic genes were downregulated (FIGURE 5A). When present, itaconate downregulated *zwf* expression in glucose-fed *P. aeruginosa* (FIGURE 5B), indicative of active catabolite repression and likely use of itaconate as main carbon source. When we analyzed a Δ*zwf* PAO1 mutant and its complemented strain Δ*zwf* Comp, we observed that lack of *zwf* function increased energy production with itaconate but not glucose or succinate (FIGURE 5C). Itaconate addition to Luria-bertani (LB) media increased growth of the Δ*zwf* PAO1 strain but not the WT or complemented control (FIGURE 5D), which correlated with increased expression of *ict*, *ich* and *ccl* (FIGURE 5E), the three genes involved in itaconate metabolism in environmental *P. aeruginosa*. Together, these findings suggested that itaconate provides *P. aeruginosa* with energy while reducing *zwf* function and shunting glucose into generation of EPS.

To test the impact of reduced glucose catabolism on immune signaling by *P. aeruginosa*, we infected mice with the Δ*zwf* PAO1 mutant and the complemented control. We observed that lack of *zwf* function only reduced IL-1β BAL accumulation, as IL-6 and TNFα remained unchanged (FIGURE 5F). Infection due to the Δ*zwf P. aeruginosa* was associated with greater numbers of alveolar macrophages (FIGURE 5G and FIGURE S4A) as it induced less cell death (FIGURE S4B). The Δ*zwf P. aeruginosa* infection conserved more Ly6C^{high}Ly6G^{-} monocytes and Ly6C$^{high/low}$Ly6G^{+} neutrophils in the BAL (FIGURE 5G and FIGURE S4C). These findings suggest that reduced glucose catabolism by *P. aeruginosa* induces less

Author Manuscript Author Manuscript Author Manuscript Author Manuscript

IL-1β-associated myeloid cell death and instead, results in a relative accumulation of phagocytes that might contribute to the release of itaconate into the airway.

P. aeruginosa clinical isolates have an unusual ability to assimilate itaconate and produce biofilm

Having found that itaconate regulates EPS-LPS dynamics on the *P. aeruginosa* surface and the relative preferences of *P. aeruginosa* from different stages of infection for myeloid metabolites, we evaluated whether host-adapted *P. aeruginosa* isolates displayed genetic and metabolic adaptation to itaconate. We reviewed the sequenced genomes of 17 CF-associated clinical isolates of *P. aeruginosa* collected over 5 years (Riquelme et al., 2019) (FIGURE 1C) and found they had accumulated non-synonymous mutations (NSM) in *lptD*, *algW* and *pelA*, but not in *algT*, *algD*, *pslA*, *ict*, *ich* and *ccl* (FIGURE 6A). In two representative isolates, mucoid 605 and small-colony variant (SCV) 686, these mutations correlated with differential mRNA expression profiles associated with outer membrane stress: *lptD* was almost undetectable, *pelA* and *pslA* were slightly upregulated and *algD* was substantially increased (FIGURE 6B). We noted that expression of the genes enabling *P. aeruginosa* to metabolize itaconate, *ict*, *ich* and *ccl*, increased in *P. aeruginosa* strains as a function of their relative adaptation to the airway: CF host-adapted strains, from additional, independent collections had substantial upregulation of these genes with respect to PAO1, whereas control acute ICU isolates, in general, did not (FIGURE 6C). These genes are at least 50% conserved at the levels of gene and protein identity in the majority of available *P. aeruginosa* genomes (FIGURE S5A–B). The *P. aeruginosa* itaconate-associated genes/proteins sequences were significantly less frequent in genomes of other common respiratory pathogens, such as *Haemophilus influenzae, Klebsiella pneumoniae, Stenotrophomonas maltophilia, Burkholderia cepacia complex, Achromobacter xylosoxidans, Acinetobacter baumanni, Staphylococcus aureus, Streptococcus pneumoniae* and *Mycobacterium* (FIGURE S5C–H). It appears that *P. aeruginosa* has a relatively unique genetic capability to induce and consume airway itaconate while modifying immunostimulatory surface components, which could be a factor in its high prevalence as a cause of major pulmonary infection.

Host-adapted *P. aeruginosa* isolates become itaconate-dependent

As itaconate is considered an antibacterial metabolite produced by myeloid cells (Naujoks et al., 2016; Rittenhouse and McFadden, 1974), we predicted that *P. aeruginosa* must be obligated to metabolize it in order to persist. The role of itaconate in supporting growth and biofilm production was tested in the phenotypically mucoid *P. aeruginosa* strain 605, which acquired resistance to multiple antibiotics in the human airway (FIGURE 6D). The upregulation of the itaconate-catabolism genes was confirmed as a response to selective pressure, as a Δ*ict* 605 isogenic mutant did not grow in glucose when itaconate was present and failed to produce biofilm (FIGURE 6E–F). While unable to grow on itaconate, in the presence of both itaconate and succinate, planktonic growth by the Δ*ict*-mutant was slightly rescued, but not the ability to form biofilm (FIGURE 6G–H). Similar findings were observed with non-adapted PAO1, as succinate, but not glucose, rescued both biofilm formation and growth by its isogenic Δ*ict* mutant (FIGURE S6A–D). The ability of *P. aeruginosa* isolates to resist itaconate toxicity was demonstrated *in vivo*, as intranasal

Author Manuscript Author Manuscript Author Manuscript Author Manuscript

administration of a high 60 mM itaconate dose barely changed the CFUs levels and did not eradicate infection from the mouse airway (FIGURE S6E). These findings suggest that the metabolic adaptation of the clinical isolates to itaconate toxicity, and likely to Enter-Duodoroff pathway suppression, had generated itaconate dependency.

Adaptation to itaconate alters the ability of *P. aeruginosa* to infect the mouse airway

We anticipated that the accrual of metabolic changes in response to itaconate toxicity would impact the infectious phenotype of *P. aeruginosa* isolates in the host lung. More than growing exponentially as laboratory strains do, host-adapted *P. aeruginosa* variants are selected as proficient biofilm producers in response to environmental stress (Maurice et al., 2018). This particular bacterial community is known for their high degree of resistance to antibiotic therapy and penetrance of immune components (Taylor et al., 2014), thus preserving a chronic reservoir of lung-adapted mutants (Driffield et al., 2008). As compared with control PAO1, we recovered fewer CFUs from WT mouse airway infected with the host-adapted strain 605 (Figure S6F). We confirmed this phenotype correlated with long-term adaptation to itaconate, as *ict* deletion from 605 rescued the number of CFUs to a level similar to infection caused by PAO1 (Figure S6F). This strong association between in-host adaptation to itaconate, metabolic reprograming and acquisition of the biofilm lifestyle was not a property of PAO1, which has never been exposed to itaconate previously. Indeed, WT and Δ*ict* PAO1 exhibited similar CFUs in the mouse airway (Figure S6G), confirming that the *in vivo* metabolic changes associated with the itaconate-*ict* axis are displayed in *P. aeruginosa* strains that also harbor the rest of these adaptive changes, in *lptD*, *algD* and *zwf*. In this context, we recapitulated the 605 infectious phenotype in PAO1 mutants lacking either *zwf* function (Δ*zwf*) (Figure S6H), *lptD* activity (Δ*lptD*4213) (Figure S6I) or expressing *algD* (Figure S6J), as each of these mutant strains caused decreased airway infection (as measured by differences in CFUs) in mice with respect to their corresponding controls. The cumulative effects of *ict* overexpression, *lptD-algD-zwf* deregulation and itaconate dependence predicted that such host-adapted *P. aeruginosa* isolates would exploit itaconate as major airway carbon source.

Itaconate-adapted *P. aeruginosa* exploit host *Irg1* function to infect the airway

To assess the overall importance of host itaconate in pathogenesis, we infected *Irg1*$^{-/-}$ mice, with either host-adapted CF strains or with PAO1, the laboratory control strain. Consistent with their acquired dependence upon itaconate consumption in the human airways, we observed that in the absence of *Irg1* there was significantly ($P < 0.0001$) decreased recovery of the host-adapted *P. aeruginosa* from lungs and the BAL (FIGURE 6I). In contrast, PAO1 infection in the *Irg1*$^{-/-}$ mice was slightly but not significantly greater than in the WT mice ($P > 0.05$) (FIGURE 6J). Correlating with their lack of *lptD*, augmented *algD* expression and substantial itaconate response in the airway (FIGURE 1C), the host-adapted strains failed to induce IL-1β in either WT or *Irg1*$^{-/-}$ mice (FIGURE 6K). Itaconate-adapted *P. aeruginosa* induced a highjacked inflammatory response that fuels infection.

Author Manuscript Author Manuscript Author Manuscript Author Manuscript

Host-adapted *P. aeruginosa* induce accumulation of itaconate-producing monocytes in the mouse airway

Itaconate is one of the most abundant metabolites produced by myeloid cells in response to infection (Lampropoulou et al., 2016). Circulating human monocytes, such as peripheral $CD14^{++}$ cells, are strong itaconate producers (Dominguez-Andres et al., 2019) and are also actively recruited into the lung during infection (Jardine et al., 2019). These $CD14^{++}$ monocytes are represented in the mouse model in part by the $Ly6C^{high}Ly6G^{-}$ population (Ingersoll et al., 2010; Narasimhan et al., 2019). Having found that the presence of alginate prevents phagocytes from IL-1β-dependent cell death and stimulates airway itaconate accumulation, we expected to see that mouse lungs infected with CF-associated *P. aeruginosa* isolates with increased *algD* expression would accumulate more Irg1-expressing $Ly6C^{high}Ly6G^{-}$ cells. From the entire monocyte population found in the host-adapted *P. aeruginosa* infected BAL, 75% corresponded to $Ly6C^{high}Ly6G^{-}$ and 25% to $Ly6C^{low}Ly6G^{-}$ cells (FIGURE 7A–B). These values substantially differed from what was observed with PBS or PAO1-treated animals, in which the majority of monocytes corresponded to $Ly6C^{low}Ly6G^{-}$ cells (FIGURE 7A–B). The importance of these differences was confirmed as we documented that 95% of the $Ly6C^{high}Ly6G^{-}$ monocytes induced by the host-adapted strains expressed Irg1, as opposed to the 60% of the monocyte population recruited by PAO1 infection (FIGURE 7C–D). No differences in Irg1 intracellular levels were observed in the $Ly6C^{low}Ly6G^{-}$ cells population for both type of bacteria (FIGURE S7A). These data suggest that host-adapted *P. aeruginosa* induce accumulation of specific airway itaconate-producing immune cells that augment the bacterium's metabolic requirements.

Subjects with CF harbor an increased population of peripheral and airway IRG1-expressing $CD14^{+}CD16^{-}$ monocytes

We next sought to determine if the analogous population of $CD14^{+}$ monocytes in humans is increased in response to *P. aeruginosa* infection. As most subjects with CF are infected with alginate-producing *P. aeruginosa* (albeit it to varying degrees), we predicted that these individuals would harbor increased numbers of circulating IRG1-expressing peripheral blood mononuclear cells (PBMCs). Analysis of monocytes among PBMCs from a third human cohort of healthy controls and adult subjects with CF confirmed a significantly increased frequency of $CD14^{++}CD16^{-}$ (classical monocytes) and $CD14^{++}CD16^{+}$ (intermediate monocytes) cells expressing high levels of IRG1 in the CF group as compared with controls (FIGURE S7B–E). No major differences were observed between controls and subjects with CF in the frequency of the $CD14^{-}CD16^{-}$ cells in PBMCs, which were found to be poor IRG1 producers (FIGURE S7C, FIGURE S7E–F). This increased frequency of circulating $IRG1^{+}CD14^{++}$ PBMCs in the majority of individuals with CF correlated with prior exposure to alginate-producing *P. aeruginosa* (FIGURE S7G).

In a fourth human cohort, we analyzed sputum from healthy subjects and individuals with CF and found that $CD14^{+}CD16^{-}$ cells predominated among all airway myeloid cells ($CD45^{+}CD19^{-}CD3^{-}$ lineage cells) in the subjects with CF (FIGURE 7E–F and FIGURE S7H). Although total alveolar macrophage numbers, depicted as $CD14^{+}CD16^{+}$ in human lungs (Jardine et al., 2019), did not change between healthy subjects and individuals with CF (FIGURE 7G and FIGURE S7I), IRG1-producing $CD14^{+}CD16^{-}$ monocytes were

Author Manuscript Author Manuscript Author Manuscript Author Manuscript

significantly increased in sputum from individuals with CF versus healthy controls (FIGURE 7H–I and FIGURE S7I). We found that accumulation of these IRG1^{+}-cells correlated with increased itaconate levels in sputum from individuals with CF with respect to controls (FIGURE 7J), probably in response to accumulation of the pro-oxidants metabolites succinate and glucose also produced by active immune cells (FIGURE 7J). Thus, individuals with CF with chronic EPS-producing *P. aeruginosa* infection exhibit more itaconate-producing cells in the blood and the airways, cells that provide a substrate that can promote persistent infections.

Amidst the pressure to develop novel antimicrobial strategies to target infection caused by multiply drug resistant opportunistic infectious agents, such as *P. aeruginosa*, there is renewed interest in identifying novel targets to suppress bacterial proliferation. In the studies presented in this report, we demonstrate one of the major challenges in targeting *P. aeruginosa*; namely, its exceptional metabolic flexibility. By studying a variety of isolates that had adapted to their human hosts, we demonstrate that a highly conserved series of genetic changes enables this species, specifically, to adapt to the consumption of itaconate. The rapid switch in cell surface display from LPS to EPS and suppression of glucose catabolism provide a feed-forward mechanism to generate itaconate. By inducing and then consuming the itaconate, which serves to protect the host from oxidant damage, *P. aeruginosa* supports a self-sustaining community of bacteria. While it is disconcerting that these bacteria can exploit the basic elements of host immune defenses for their own benefit, controlling acute inflammation and the abundance of favored metabolites could reduce the risk of developing intractable long-term infection.

Alginate is synthetized in varying degrees in many clinical settings of *P. aeruginosa* infection (Bragonzi et al., 2005; Hentzer et al., 2001), in addition in the lungs of individuals with CF. Its production correlates with the intensity of the oxidative response mounted by the host. Unexpectedly, we found that alginate has important immunoregulatory functions for host immune cells. Far from an inert protective shell for the bacteria, alginate induces metabolic changes in myeloid cells, changes that are also dictated by LPS and associated with how cells produce energy during infection (Mills et al., 2016). Macrophage metabolic reprograming in response to LPS increases production of itaconate (Lampropoulou et al., 2016), which we confirmed here *in vivo* with alginate-producing bacteria. By studying a variety of clinical isolates, including those that have undergone selection for persistence in the setting of airway inflammation, as in our CF-associated strains, we noted the emergence of mutants that by limiting the generation of IL-1β, they prevented myeloid cell death and induced more airway itaconate. The CF-associated isolates provide the opportunity to determine the long-term effects of bacterial adaptation to the inflamed airway, changes that are ongoing but less obvious in other settings. While the acute LPS-TLR4-mediated inflammatory response is a key component of initial infection, the rapid endotoxin-TLR4 signaling suppression and active EPS-mediated oxidative macrophage metabolism provides a complex mechanism of pathogenesis that favors long-term infection by *P. aeruginosa*. The contribution of host immunity to infection should be considered in the future development of next-generation antibacterial therapies.

Author Manuscript Author Manuscript Author Manuscript Author Manuscript

Increasing evidence suggests that during infection, immunometabolites induce key post-translational modifications in proteins and metabolites involved in host immunity. Whereas succinate produces protein lysine succinylation in several metabolic pathways primed by LPS (Tannahill et al., 2013), itaconate induces Keap1 alkylation (Mills et al., 2018) and glutathione electrophilic stress (Bambouskova et al., 2018), major regulators of the *Nrf2* antioxidant response. The progressive accumulation of these metabolites in the airway and chronic exposure of *P. aeruginosa* to them likely induces clinically relevant modifications in bacterial gene products associated with intractable infection. LPS trafficking and its display on the outer membrane rely on key cysteine-to-cysteine interactions within the LptD core (Ruiz et al., 2010), and the potential of itaconate to modify these thiol groups might favor membrane stress and activation of the *algT* anti-stress response, as we observed here. The explicit role of immunometabolites on the modification of bacterial macromolecules remains to be evaluated.

The acute pro-inflammatory response evoked by environmental and laboratory *P. aeruginosa* strains compromises host survival and limits the long-term metabolic evolution predicted to occur in these bacteria (Riquelme et al., 2017; Riquelme et al., 2019; Winstanley et al., 2016). The use of host-adapted clinical isolates that have been selected over years of exposure to the oxidative environment in the inflamed human airway provides a more nuanced model of infection to study how *P. aeruginosa* exploits immune components to cause chronic disease. The accumulation of itaconate-producing $CD14^+$ myeloid “feeder” cells into the infected lungs provides a reliable energy source for host-adapted bacteria. The availability of mouse models that elicit the same population of myeloid feeder cells might provide a useful tool to identify future therapeutic strategies to treat aggressive *P. aeruginosa* infections. Indeed, while there has been substantial alarm raised by the spectrum of multiply antibiotic resistant strains of bacteria, particularly *P. aeruginosa*, by identifying the mechanisms by which these organisms adapt and exploit host immune defenses it is conceivable that future therapies could be developed that target these very adaptations to combat such infectious agents and the devastating diseases they cause.

Limitations of Study

We acknowledge that the complex metabolic matrix of the inflamed human airway might not be fully represented by mouse models of pneumonia. *In situ* concentrations of metabolites in the airway of mice and in healthy individuals or individuals with CF might differ due to different degrees of dehydration, mucus accumulation, myeloid cell activities and phagocyte numbers. These variables must be better characterized in future work. Further, the intricate metabolic program exhibited by *P. aeruginosa* isolates suggests that metabolites other than itaconate might also be fueling their in-host selection. Our study does not consider the interactions between itaconate and other pathways, providing only a partial mechanism of the chronic CF-associated infectious pathology. Our studies are also limited by determining *in vitro* but not *in vivo* the gene expression program of *P. aeruginosa* in the presence of itaconate. We extrapolate data using laboratory *P. aeruginosa* and mouse strains to findings observed in *P. aeruginosa* mutants derived from chronically infected patients. A more comprehensive study with a further diverse collection of *P. aeruginosa* isolates and human cells would support and improve the conclusions of this manuscript.

Author Manuscript Author Manuscript Author Manuscript Author Manuscript

STAR METHODS

● RESOURCE AVAILABILITY

Lead contact—● Further information and requests for resources and reagents should be directed to and will be fulfilled by the Lead Contact, Dr. Alice Prince (asp7@cumc.columbia.edu).

Materials availability—● *P. aeruginosa* clinical isolates and mutants analyzed in this work are available from the Lead Contact without restriction.

Data and Code Availability—● The published article includes all datasets generated or analyzed during this study.

● EXPERIMENTAL MODEL AND SUBJECT DETAILS

Human Samples—All human blood samples from healthy individuals and subjects with CF were obtained from adults in the CF program at Columbia University under the IRB AAAR1395 approved protocol. Male and female samples were collected in an approximate 50%−50% ratio. Under the clinical settings of this study, age and gender are not expected to influence the variables tested. Sputum samples from healthy adult individuals and subjects with CF were provided by Dr. Clemente Britto-Leon from Yale University. In total, 23 CF and 19 healthy control samples were studied. An informed consent was signed by all subjects providing samples.

Mice experiments –: All animal experiments were performed following institutional guidelines at Columbia University. Animals were housed and maintained at Columbia University Irving Medical Center under regular rodent light/dark cycles, 18–23°C, as well as fed with regular irradiated chow diet (Purina Cat 5053, distributed by Fisher). Mice health was routinely checked by an institutional Veterinary. Mice studies were approved by protocol IACUC AAAR9403 and IACUC AABE8600. 6–8-week-old (20–25grs) WT C57bl/6 mice were obtained from The Jackson Laboratories. *Irg1*$^{-/-}$ (*Acod1*$^{-/-}$) were also obtained from The Jackson Laboratories and bred in our facilities, Columbia University Irving Medical Center. These mice were used between 6–8-week-old. WT and *Irg1*$^{-/-}$ mice are immunocompetent animals, and they received neither medical nor drug treatments previous to infection experiments. Each *in vivo* experiment was performed using 50% female and 50% male animals. Sex was not expected to influence the final results of experiments. During studies, animals were randomly assigned to cages. For experiments using bone-marrow derived macrophages (BMDMs), 50% of experiments were done using males and the other 50% females.

***P. aeruginosa* strains–:** Laboratory *P. aeruginosa* strains used in this study were: WT PA14, WT PAO1, Δ*zwf* PAO1, Δ*zwf* complemented PAO1, Δ*algD* PAO1, Δ*lptD*4213 PAO1. Clinical *P. aeruginosa* strains used were: 17 host-adapted *P. aeruginosa* strains recovered between 2012–2015 from sputum of a chronic-infected CF patient (Riquelme et al., 2019) (“CF Patient 3”); 3 “CF Patient 1” strains collected from a 5 year-old chronically infected CF patient; 3 “CF Patient 2” strains collected from a 10 year-old chronically CF infected

Author Manuscript Author Manuscript Author Manuscript Author Manuscript

patient; 10 ICU isolates were obtained from 10 acutely infected patients at Columbia University Irving Medical Center facilities. All of these strains were plated in LB agar and their phenotypes were characterized regarding SCV and mucoid morphology. For overnight and kinetic growth studies in minimal media with different carbon sources, overnight LB-cultured *P. aeruginosa* strains were extensively washed and subcultured in complete M9 minimal media supplemented or not with 62.5mM itaconate, glucose or succinate (pH 7.0). For overnight growth studies, culture was performed under agitation in 96-well plate, and 16h later growth was measured at $OD600_{nm}$. For kinetic studies, strains were inoculated in 96-well plates and growth was studied at 37°C. When mentioned, LB-cultured PAO1, Δ*zwf* and Δ*zwf* complemented PAO1 were growth overnight in LB supplemented or not with increasing itaconate concentrations. Overnight OD_{600} was measured as growth. For mice infection studies, all strains were culture overnight in LB, then subcultured until exponential growth, extensively washed and used to infect animals.

● METHOD DETAILS

Human PBMCs flow cytometry ––Fresh blood samples obtained from randomly selected individuals were centrifuged in BD Vacutainer CPT tubes and the PBMCs-containing buffy coat was recovered. Buffy coat was washed several times in PBS and resuspended in FACS buffer. Cells were stained extracellularly for CD14, CD15, CD11b, CD45, CD19, CD3 and CD16. Cells were also stained for viability using DAPI live/dead kit. Once stained for 30min on ice, cells were washed and fixed/permeabilized using the Invitrogen fix/perm kit. Then, cells were stained for IRG1 with a rabbit monoclonal antibody and then treated with a secondary antibody anti rabbit coupled to AF647. Staining was for 30 min each, and then cells were washed extensively and fixed with 2% PFA-PBS. Cells were analyzed by flow cytometry LSRII machine and analyzed with FlowJo X.

Human Sputum flow cytometry ––Sputum samples from randomly selected patients were digested with DTT 0.1 % 10mM Sodium Acetate for 30min on ice with intermittent vortexing. Samples were passed through a sterile gaze and filtered through a 40umts cell strainer. Single cell solutions were centrifuged and washed 3 times with RPMI. Then, cells were stained extracellularly for CD14, CD15, CD11b, CD45, CD19, CD3 and CD16 and also stained for viability using DAPI live/dead kit. Once stained for 30min on ice, cells were washed and fixed/permeabilized using the Invitrogen fix/perm kit. The, cells were stained for IRG1 with a rabbit monoclonal antibody and then treated with a secondary antibody anti rabbit coupled to AF647. Staining was for 30min each, and then cells were washed extensively and fixed with 2% PFA-PBS. Cells were analyzed by flow cytometry and analyzed with FlowJo X.

Itaconate *P. aeruginosa* mutants generation ––The itaconate mutant strains in this study were created in the *Pseudomonas aeruginosa* PAO1 and host-adapted 605 strain backgrounds using homologous recombination. Constructs for these deletions were generated using the yeast gap repair cloning method and employed the allelic-replacement vector pMQ30 and the yeast strain InvSc1. For deletion of a specific gene, ~1 kb flanking regions plus ~100 bp of each end of the coding region were amplified and cloned into the plasmid. Resultant plasmids were propagated in *E. coli* UQ950, transformed into the mating

Author Manuscript Author Manuscript Author Manuscript Author Manuscript

strain *E. coli* BW29427, and transferred into PAO1 and 605 strain by conjugation. Recombinants were plated onto selective media containing 100 μg/mL gentamicin. Candidate mutant strains were identified by counter-selection on LB agar containing 10% sucrose without NaCl. Verification of the final clones was obtained via PCR and sequencing.

LPS Studies ––To visualize the O-antigen and core ladder of bacteria, LPS was first isolated using a hot phenol extraction from overnight cultures normalized to OD_{600} of 0.5 after 1:10 dilution. Samples were treated with DNase and RNase for 30 min at 37°C and Proteinase K at 59°C overnight. After hot phenol extraction with Trizol, the isolated LPS was run on a Tricine 10–20% gel. The gel was then stained using Pro-Q Emerald 300 Lipopolysaccharide Gel Stain Kit and imaged using UV light on a Protein Simple imager.

LPS detection in Δ*lptD*4213 PAO1 strains ––Both WT and Δ*lptD*4213 PAO1 were grown overnight in LB, washed extensively with PBS and stained with two anti-LPS carbohydrates antibodies for 30min. Then, cells were washed and stained with anti H+L-mouse IgM AF 598. Cells were analyzed by flow cytometry.

Biofilms studies with *P. aeruginosa* strains ––Isolates and laboratory controls were growth in LB overnight, extensively washed in minimal media and then inoculated in 96-well plates containing different carbon sources in M9-Salts supplemented. Plates were incubated under agitation at 37°C overnight. Next day, bacterial growth was measured at OD_{600nm}, supernatant discarded and then stained for biofilm with crystal violet (CV). Biofilm production was analyzed at OD_{540nm}.

***P. aeruginosa* membrane potential ––**PAO1 was grown overnight in LB under agitation. Then, bacteria were extensively washed in M9 media and added to M9 supplemented either with glucose or glucose + itaconate (60mM each). After overnight incubation, bacteria were washed and incubated with *bac*light $DiOC_2(3)$ dye and analyzed by flow cytometry as indicated by the manufacturer. Membrane potential was calculated as the ratio between red and green $DiOC_2(3)$ fluorescence in the green positive population. Forward (bacterial size) and Side (surface granularity) scatters were measured as well.

Carbon source assimilation by *P. aeruginosa* ––Either PAO1, Δ*zwf* and its complemented counterpart were grown until exponential phase, OD_{600nm} measured and applied at same concentration to a 96-well plate array where each well contained a single carbon source (PM1 and PM2A plates). For preparation of bacteria, solutions and plates the instructions of the manufacturer were followed. Plates were incubated at 37°C for 48h-72h.

Mice infection with *P. aeruginosa* strains ––When indicated, either PAO1, Δ*lptD*4213 PAO1, Δ*zwf* PAO1, Δ*zwf* complemented PAO1, Δ*algD* PAO1, Δ*ict* PAO1, control 605, Δ*ict* 605, or a mix of all 17CF isolates were used to infect either WT and/or *irg1*$^{-/-}$ (*Acod1*$^{-/-}$) C57bl/6 mice. Mice were infected with 50uL PBS containing total 10^7 CFU or PBS alone (non-infected) (in the mix of 17CF strains, equal parts of 5.9×10^5 for each were used). 16h later, mice were sacrificed and BAL and lungs were collected. CFU amounts (LB agar plating), as well as immune cells (flow cytometry) and cytokines (ELISA) were quantified in BAL and in lungs. Flow cytometry; alveolar macrophages

Author Manuscript Author Manuscript Author Manuscript Author Manuscript

($CD45^+CD11b^{low/-}SiglecF^{high}CD11c^+CD193^-Ly6G^-Ly6C^-$), neutrophils ($CD45^+CD11b^{high}SiglecF^{low/-}CD11c^-MHCII^-CD193^-Ly6G^+Ly6C^{low/-}$) and monocytes ($CD45+CD11b^{high}SiglecF^{low/-}CD11c^-MHCII^-CD193^-Ly6G^-Ly6C^{low/high}$). Samples were analyzed with FlowJo X. Cell viability was determined by using live/dead DAPI staining. When indicated, BAL were analyzed by Mass-Spec metabolomics for succinate, glucose and itaconate abundance in all treatments.

***In vivo* Itaconate administration** ––WT C57bl/6 mice were intranasally infected with 10^7 CFU of the collection of 17 CF *P. aeruginosa* isolates (equal parts of 5.9×10^5 for each strain). 24h later, mice were anesthetized and treated intranasally with 50uL of 60mM itaconate, pH 7. Mice were sacrificed 24h later and CFUs were quantified in lungs and BALs.

Seahorse experiments ––Mouse BMDMs were infected for 3h at multiplicity of infection (MOI)=10 with either PAO1, Δ*algD* or Δ*lptD*4213 strains. When indicated, cells were treated only with PBS, 50ug/ml LPS, 50ug/ml of soluble alginate, 50ug/ml of polyethylene glycol (PEG, 200, 8000, 20000 MW) or 50ug/ml N-acetyl Glucosamine. During the infection cells were analyzed in a Seahorse machine using commercially obtained plates as recommended by the manufacturer to evaluate glycolysis (ECAR) and the oxygen consumption rate (OCR).

Mitochondrial studies in macrophages ––Mouse BMDMs were infected at 37°C for 2h at multiplicity of infection (MOI)=10 with either PAO1, Δ*algD* or Δ*lptD*4213 strains. When indicated, cells were treated only with PBS, 50ug/ml LPS or 50ug/ml of soluble alginate. Then, cells were extensively washed and stained for mitochondrial membrane potential with Dilc1(5) and mitochondrial ROS ($O_2{*}^-$) with Mitosox dyes. Cells were extensively washed, resuspended in PBS and analyzed in a FACs CantoII flow cytometry machine. Data was analyzed with Flowjo X.

Whole genome comparison for metabolic genes ––Three genes of interest in PAO1 were studied: *ict* (PA0878), *ich* (PA0882) and *ccl* (PA0883). Both gene and protein coverage and identity for each of these metabolic regulators were searched and compared using Blast (https://blast.ncbi.nlm.nih.gov/Blast.cgi) against the whole database of genomes published and available online. Taxid used for each pathogen was: *P. aeruginosa* (taxid 136841); *H. influenza* (taxid 727); *B. cepacia complex* (taxid 87882); *S. maltophilia* (taxid 995085); *A. xylosoxidans* (taxid 85698); *A. baumanni* (taxid 470); *Mycobacterium* (taxid 85007); *K. pneumoniae* (taxid 573); *S. pneumoniae* (taxid 1313); *S. aureus* (taxid 1280). Coverage and identity obtained were graphed and analyzed.

Airway metabolomics ––BAL from either non-infected or 16h-infected mice were collected with 3ml of sterile PBS. Samples were immediately placed on ice. Then, samples were diluted with 100% methanol in a 1:1 proportion, mixed and stored at −80C for future metabolomics analysis. Just prior to mass spectrometry, samples were thawed and dried under a stream of N_2 and were resuspended in HPLC-grade water at a 4:1 dilution (relative to the original BAL volume). High-resolution mass spectrometry data were acquired on a Thermo Fisher Exactive Mass spectrometer in negative mode using 25 min reverse phase

Author Manuscript Author Manuscript Author Manuscript Author Manuscript

gradients and ion-pairing chromatography. Metabolites were identified using the known chromatographic retention times of standards, and metabolite signals were quantified using MAVEN. Metabolite signal intensities were used to quantify difference between treatments in BAL and respect to PBS-treated animals.

qRT-PCR for genes in *P. aeruginosa* ––PAO1 strains were grown ON in LB and then subcultured in LB, or M9 supplemented with succinate, glucose or itaconate (50 mM) until exponential phase. Total RNA was extracted using either the RNeasy Mini Kit or the E.Z.N.A. Total RNA Kit 1. The RNA was then treated with DNase (DNA-free kit). The RNA concentration was measured using a NanoDrop One. cDNA was synthesized using High Capacity cDNA Reverse Transcription Kit (Applied Biosystems), and qPCR was performed with a StepOnePlus Real-Time PCR System (Applied Biosystems) using POWER SYBR Green PCR Master Mix (Applied Biosystems). Sequences of the primers used for qRT-PCRs are listed in Star Methods Key Resource Table. Relative gene expression was calculated by the $2^{-\Delta\Delta CT}$ method. The *rpsL* gene was used as a reference housekeeping gene, and the *P. aeruginosa* PAO1 strain grown in LB was used as a calibrator.

● QUANTIFICATION AND STATISTICAL ANALYSIS

Statistical analysis ––We modelled the amounts of independent experiments required to reach significance between groups by using the computer program JMP. Also, we based this simulation on experimental design, preliminary data and past experience. These analyses were done assuming a 20% standard deviation, and equivalent variances within groups. Significance < 0.05 with power 0.8 was used. Experiments in this study were not performed in a blinded fashion. Exclusion criteria: Analysis of blood and sputum did not include children samples, as mostly adults experience chronic *P. aeruginosa* infection. Out of the total number of human samples analyzed, 100% corresponded to adults. All analyses and graphs were performed using the GraphPad Prism 7a and 8 software. Data in graphs are shown as average +/− SEM and data were assumed to follow a normal distribution. For comparison between average values for more than 2 groups, we performed One-Way ANOVA with a multiple posteriori comparison. When studying two or more group along time, data was analyzed using Two-Way ANOVA with a multiple posteriori comparison. Differences between two groups in samples' average values were analyzed using analysis of variance (parametric) or Student's *t*-test for normally distributed data or Mann-Whitney or Kruskal-Wallis test otherwise. Differences were considered significant when P value (two-sides) was under 0.05 ($P < 0.05$). Significances P values and amount of independent experiments and replicates are indicated in each Figure Legend.

● ADDITIONAL RESOURCES

This study does not have additional resources.

Supplementary Material

Refer to Web version on PubMed Central for supplementary material.

Author Manuscript Author Manuscript Author Manuscript Author Manuscript

Acknowledgments:

We thank Drs. Ian Lewis and Ryan Groves for their support in metabolomics studies; Dr. Joanna Goldberg for providing the *algD* PAO1 mutant and her helpful discussions; Dr. Carl J. Balibar for providing us with the Δ*lptD*4213 PAO1 mutant strains; Dr. Dennis E. Ohman for sharing with us Δ*zwf* and Δ*zwf* Comp PAO1 strains; Dr. William Sieling for human blood sampling.

Funding: A.P. is supported by NIH 1R35HL135800 and by Integrating Special Populations (ISP) Resource, CTSA, Columbia University (GG011557-26); SR by a CFF Postdoctoral fellowship RIQUEL 17F0/PG008837; CL by S. B. Postdoct Contract CD15/00125 and M-AES mobility grant MV16/00053; This publication by the NCATS-NIH, UL1TR001873 and by FIS PI16/01381 from ISCIII and performed in the CCTI Flow Cytometry Core at CUMC, NIH (S10RR027050).

References

Arai H (2011). Regulation and Function of Versatile Aerobic and Anaerobic Respiratory Metabolism in *Pseudomonas aeruginosa*. Front Microbiol 2, 103. [PubMed: 21833336]

Balibar CJ, and Grabowicz M (2016). Mutant Alleles of lptD Increase the Permeability of *Pseudomonas aeruginosa* and Define Determinants of Intrinsic Resistance to Antibiotics. Antimicrob Agents Chemother 60, 845–854. [PubMed: 26596941]

Bambouskova M, Gorvel L, Lampropoulou V, Sergushichev A, Loginicheva E, Johnson K, Korenfeld D, Mathyer ME, Kim H, Huang LH, et al. (2018). Electrophilic properties of itaconate and derivatives regulate the IkappaBzeta-ATF3 inflammatory axis. Nature 556, 501–504. [PubMed: 29670287]

Botos I, Majdalani N, Mayclin SJ, McCarthy JG, Lundquist K, Wojtowicz D, Barnard TJ, Gumbart JC, and Buchanan SK (2016). Structural and Functional Characterization of the LPS Transporter LptDE from Gram-Negative Pathogens. Structure 24, 965–976. [PubMed: 27161977]

Bragonzi A, Worlitzsch D, Pier GB, Timpert P, Ulrich M, Hentzer M, Andersen JB, Givskov M, Conese M, and Doring G (2005). Nonmucoid *Pseudomonas aeruginosa* expresses alginate in the lungs of patients with cystic fibrosis and in a mouse model. J Infect Dis 192, 410–419. [PubMed: 15995954]

Collier DN, Hager PW, and Phibbs PV Jr. (1996). Catabolite repression control in the *Pseudomonads*. Res Microbiol 147, 551–561. [PubMed: 9084769]

Cornforth DM, Dees JL, Ibberson CB, Huse HK, Mathiesen IH, Kirketerp-Moller K, Wolcott RD, Rumbaugh KP, Bjarnsholt T, and Whiteley M (2018). *Pseudomonas aeruginosa* transcriptome during human infection. Proc Natl Acad Sci U S A 115, E5125–E5134. [PubMed: 29760087]

Deretic V, Schurr MJ, and Yu H (1995). *Pseudomonas aeruginosa*, mucoidy and the chronic infection phenotype in cystic fibrosis. Trends Microbiol. 3, 351–356. [PubMed: 8520888]

Dhar S, Kumari H, Balasubramanian D, and Mathee K (2018). Cell-wall recycling and synthesis in *Escherichia coli* and *Pseudomonas aeruginosa* - their role in the development of resistance. J Med Microbiol 67, 1–21. [PubMed: 29185941]

Dominguez-Andres J, Novakovic B, Li Y, Scicluna BP, Gresnigt MS, Arts RJW, Oosting M, Moorlag S, Groh LA, Zwaag J, et al. (2019). The Itaconate Pathway Is a Central Regulatory Node Linking Innate Immune Tolerance and Trained Immunity. Cell Metab 29, 211–220 e215. [PubMed: 30293776]

Driffield K, Miller K, Bostock JM, O'Neill AJ, and Chopra I (2008). Increased mutability of *Pseudomonas aeruginosa* in biofilms. J Antimicrob Chemother 61, 1053–1056. [PubMed: 18256114]

Elborn JS (2016). Cystic fibrosis. Lancet 388, 2519–2531. [PubMed: 27140670]

Evans DJ, Pier GB, Coyne MJ Jr., and Goldberg JB (1994). The rfb locus from *Pseudomonas aeruginosa* strain PA103 promotes the expression of O antigen by both LPS-rough and LPS-smooth isolates from cystic fibrosis patients. Mol Microbiol 13, 427–434. [PubMed: 7527892]

Evavold CL, Ruan J, Tan Y, Xia S, Wu H, and Kagan JC (2018). The Pore-Forming Protein Gasdermin D Regulates Interleukin-1 Secretion from Living Macrophages. Immunity 48, 35–44 e36. [PubMed: 29195811]

Author Manuscript Author Manuscript Author Manuscript Author Manuscript

Faure E, Mear JB, Faure K, Normand S, Couturier-Maillard A, Grandjean T, Balloy V, Ryffel B, Dessein R, Chignard M, et al. (2014). *Pseudomonas aeruginosa* type-3 secretion system dampens host defense by exploiting the NLRC4-coupled inflammasome. Am J Respir Crit Care Med 189, 799–811. [PubMed: 24555512]

Fernandez-Barat L, Ferrer M, De Rosa F, Gabarrus A, Esperatti M, Terraneo S, Rinaudo M, Li Bassi G, and Torres A (2017). Intensive care unit-acquired pneumonia due to *Pseudomonas aeruginosa* with and without multidrug resistance. J Infect 74, 142–152. [PubMed: 27865895]

Franklin MJ, Nivens DE, Weadge JT, and Howell PL (2011). Biosynthesis of the *Pseudomonas aeruginosa* Extracellular Polysaccharides, Alginate, Pel, and Psl. Front. Microbiol 2, 167. [PubMed: 21991261]

Garcia-Nunez M, Marti S, Puig C, Perez-Brocal V, Millares L, Santos S, Ardanuy C, Moya A, Linares J, and Monso E (2017). Bronchial microbiome, PA biofilm-forming capacity and exacerbation in severe COPD patients colonized by *P. aeruginosa*. Future Microbiol 12, 379–392. [PubMed: 28339291]

Goldberg JB, Coyne MJ Jr., Neely AN, and Holder IA (1995). Avirulence of a Pseudomonas aeruginosa algC mutant in a burned-mouse model of infection. Infect Immun 63, 4166–4169. [PubMed: 7558335]

Gorke B, and Stulke J (2008). Carbon catabolite repression in bacteria: many ways to make the most out of nutrients. Nat Rev Microbiol 6, 613–624. [PubMed: 18628769]

Hentzer M, Teitzel GM, Balzer GJ, Heydorn A, Molin S, Givskov M, and Parsek MR (2001). Alginate overproduction affects *Pseudomonas aeruginosa* biofilm structure and function. J Bacteriol 183, 5395–5401. [PubMed: 11514525]

Ingersoll MA, Spanbroek R, Lottaz C, Gautier EL, Frankenberger M, Hoffmann R, Lang R, Haniffa M, Collin M, Tacke F, et al. (2010). Comparison of gene expression profiles between human and mouse monocyte subsets. Blood 115, e10–19. [PubMed: 19965649]

Jabir MS, Hopkins L, Ritchie ND, Ullah I, Bayes HK, Li D, Tourlomousis P, Lupton A, Puleston D, Simon AK, et al. (2015). Mitochondrial damage contributes to *Pseudomonas aeruginosa* activation of the inflammasome and is downregulated by autophagy. Autophagy 11, 166–182. [PubMed: 25700738]

Jardine L, Wiscombe S, Reynolds G, McDonald D, Fuller A, Green K, Filby A, Forrest I, Ruchaud-Sparagano MH, Scott J, et al. (2019). Lipopolysaccharide inhalation recruits monocytes and dendritic cell subsets to the alveolar airspace. Nat Commun 10, 1999. [PubMed: 31040289]

Juarez P, Jeannot K, Plesiat P, and Llanes C (2017). Toxic Electrophiles Induce Expression of the Multidrug Efflux Pump MexEF-OprN in *Pseudomonas aeruginosa* through a Novel Transcriptional Regulator, CmrA. Antimicrob Agents Chemother 61.

Kim J, Jeon CO, and Park W (2008). Dual regulation of zwf-1 by both 2-keto-3-deoxy-6-phosphogluconate and oxidative stress in *Pseudomonas putida*. Microbiology 154, 3905–3916. [PubMed: 19047757]

Kubes JN, and Fridkin SK (2019). Factors affecting the geographic variability of antibiotic-resistant healthcare-associated infections in the United States using the CDC Antibiotic Resistance Patient Safety Atlas. Infect Control Hosp Epidemiol 40, 597–599. [PubMed: 30975229]

Lampropoulou V, Sergushichev A, Bambouskova M, Nair S, Vincent EE, Loginicheva E, Cervantes-Barragan L, Ma X, Huang SC, Griss T, et al. (2016). Itaconate Links Inhibition of Succinate Dehydrogenase with Macrophage Metabolic Remodeling and Regulation of Inflammation. Cell Metab 24, 158–166. [PubMed: 27374498]

Lee J, Xue M, Wzorek JS, Wu T, Grabowicz M, Gronenberg LS, Sutterlin HA, Davis RM, Ruiz N, Silhavy TJ, et al. (2016). Characterization of a stalled complex on the beta-barrel assembly machine. Proc Natl Acad Sci U S A 113, 8717–8722. [PubMed: 27439868]

Lima S, Guo MS, Chaba R, Gross CA, and Sauer RT (2013). Dual molecular signals mediate the bacterial response to outer-membrane stress. Science 340, 837–841. [PubMed: 23687042]

Ma JF, Hager PW, Howell ML, Phibbs PV, and Hassett DJ (1998). Cloning and characterization of the *Pseudomonas aeruginosa zwf* gene encoding glucose-6-phosphate dehydrogenase, an enzyme important in resistance to methyl viologen (paraquat). J. Bacteriol 180, 1741–1749. [PubMed: 9537370]

Author Manuscript Author Manuscript Author Manuscript Author Manuscript

Maleki S, Maerk M, Valla S, and Ertesvag H (2015). Mutational Analyses of Glucose Dehydrogenase and Glucose-6-Phosphate Dehydrogenase Genes in *Pseudomonas fluorescens* Reveal Their Effects on Growth and Alginate Production. Appl Environ Microbiol 81, 3349–3356. [PubMed: 25746989]

Maurice NM, Bedi B, and Sadikot RT (2018). *Pseudomonas aeruginosa* Biofilms: Host Response and Clinical Implications in Lung Infections. Am J Respir Cell Mol Biol 58, 428–439. [PubMed: 29372812]

Mills EL, Kelly B, Logan A, Costa ASH, Varma M, Bryant CE, Tourlomousis P, Dabritz JHM, Gottlieb E, Latorre I, et al. (2016). Succinate Dehydrogenase Supports Metabolic Repurposing of Mitochondria to Drive Inflammatory Macrophages. Cell 167, 457–470 e413. [PubMed: 27667687]

Mills EL, Kelly B, and O'Neill LAJ (2017). Mitochondria are the powerhouses of immunity. Nat Immunol 18, 488–498. [PubMed: 28418387]

Mills EL, Ryan DG, Prag HA, Dikovskaya D, Menon D, Zaslona Z, Jedrychowski MP, Costa ASH, Higgins M, Hams E, et al. (2018). Itaconate is an anti-inflammatory metabolite that activates Nrf2 via alkylation of KEAP1. Nature 556, 113–117. [PubMed: 29590092]

Narasimhan PB, Marcovecchio P, Hamers AAJ, and Hedrick CC (2019). Nonclassical Monocytes in Health and Disease. Annu Rev Immunol 37, 439–456. [PubMed: 31026415]

Naujoks J, Tabeling C, Dill BD, Hoffmann C, Brown AS, Kunze M, Kempa S, Peter A, Mollenkopf HJ, Dorhoi A, et al. (2016). IFNs Modify the Proteome of Legionella-Containing Vacuoles and Restrict Infection Via IRG1-Derived Itaconic Acid. PLoS Pathog 12, e1005408. [PubMed: 26829557]

O'Toole GA, Gibbs KA, Hager PW, Phibbs PV Jr., and Kolter R (2000). The global carbon metabolism regulator Crc is a component of a signal transduction pathway required for biofilm development by *Pseudomonas aeruginosa*. J. Bacteriol 182, 425–431. [PubMed: 10629189]

Qin W, Qin K, Zhang Y, Jia W, Chen Y, Cheng B, Peng L, Chen N, Liu Y, Zhou W, et al. (2019). S-glycosylation-based cysteine profiling reveals regulation of glycolysis by itaconate. Nat Chem Biol 15, 983–991. [PubMed: 31332308]

Riquelme SA, Hopkins BD, Wolfe AL, DiMango E, Kitur K, Parsons R, and Prince A (2017). Cystic Fibrosis Transmembrane Conductance Regulator Attaches Tumor Suppressor PTEN to the Membrane and Promotes Anti *Pseudomonas aeruginosa* Immunity. Immunity 47, 1169–1181 e1167. [PubMed: 29246444]

Riquelme SA, Lozano C, Moustafa AM, Liimatta K, Tomlinson KL, Britto C, Khanal S, Gill SK, Narechania A, Azcona-Gutierrez JM, et al. (2019). CFTR-PTEN-dependent mitochondrial metabolic dysfunction promotes *Pseudomonas aeruginosa* airway infection. Sci Transl Med 11.

Rittenhouse JW, and McFadden BA (1974). Inhibition of isocitrate lyase from *Pseudomonas indigofera* by itaconate. Arch Biochem Biophys 163, 79–86. [PubMed: 4852477]

Rojo F (2010). Carbon catabolite repression in Pseudomonas : optimizing metabolic versatility and interactions with the environment. FEMS Microbiol. Rev 34, 658–684. [PubMed: 20412307]

Ruiz N, Chng SS, Hiniker A, Kahne D, and Silhavy TJ (2010). Nonconsecutive disulfide bond formation in an essential integral outer membrane protein. Proc Natl Acad Sci U S A 107, 12245–12250. [PubMed: 20566849]

Sasikaran J, Ziemski M, Zadora PK, Fleig A, and Berg IA (2014). Bacterial itaconate degradation promotes pathogenicity. Nat Chem Biol 10, 371–377. [PubMed: 24657929]

Tannahill GM, Curtis AM, Adamik J, Palsson-McDermott EM, McGettrick AF, Goel G, Frezza C, Bernard NJ, Kelly B, Foley NH, et al. (2013). Succinate is an inflammatory signal that induces IL-1beta through HIF-1alpha. Nature 496, 238–242. [PubMed: 23535595]

Taylor PK, Yeung AT, and Hancock RE (2014). Antibiotic resistance in *Pseudomonas aeruginosa* biofilms: towards the development of novel anti-biofilm therapies. J Biotechnol 191, 121–130. [PubMed: 25240440]

Turner KH, Everett J, Trivedi U, Rumbaugh KP, and Whiteley M (2014). Requirements for *Pseudomonas aeruginosa* acute burn and chronic surgical wound infection. PLoS Genet 10, e1004518. [PubMed: 25057820]

Wang H, Fedorov AA, Fedorov EV, Hunt DM, Rodgers A, Douglas HL, Garza-Garcia A, Bonanno JB, Almo SC, and de Carvalho LPS (2019). An essential bifunctional enzyme in *Mycobacterium*

Author Manuscript Author Manuscript Author Manuscript Author Manuscript

tuberculosis for itaconate dissimilation and leucine catabolism. Proc Natl Acad Sci U S A 116, 15907–15913. [PubMed: 31320588]

Winstanley C, O'Brien S, and Brockhurst MA (2016). *Pseudomonas aeruginosa* Evolutionary Adaptation and Diversification in Cystic Fibrosis Chronic Lung Infections. Trends. Microbiol 24, 327–337. [PubMed: 26946977]

Wongsaroj L, Saninjuk K, Romsang A, Duang-Nkern J, Trinachartvanit W, Vattanaviboon P, and Mongkolsuk S (2018). *Pseudomonas aeruginosa* glutathione biosynthesis genes play multiple roles in stress protection, bacterial virulence and biofilm formation. PLoS One 13, e0205815. [PubMed: 30325949]

World-Health-Organization (2017). Guidelines for the Prevention and Control of Carbapenem-Resistant Enterobacteriaceae, *Acinetobacter baumannii* and *Pseudomonas aeruginosa* in Health Care Facilities. (Geneva).

Wunderink RG, and Waterer G (2017). Advances in the causes and management of community acquired pneumonia in adults. BMJ 358, j2471. [PubMed: 28694251]

Author Manuscript Author Manuscript Author Manuscript Author Manuscript

Highlights

- *P. aeruginosa*-infected macrophages produce itaconate
- Itaconate generates membrane stress in *P. aeruginosa*
- Itaconate leads to decreased LPS, but increased EPS, to promote biofilm formation
- The EPS-itaconate axis thwarts immune clearance enabling chronic infection

Author Manuscript Author Manuscript Author Manuscript Author Manuscript

Context and Significance

Intractable respiratory infections remain a major public health threat. *P. aeruginosa* pneumonia, which is associated with both acute and especially chronic infections, is specially challenging and one that can acquire resistance to virtually all available antibiotics. Here, Sebastián Riquelme and colleagues describe how itaconate, a major macrophage metabolite, selects for a reservoir of highly adapted *P. aeruginosa* mutants capable of producing biofilm in the lung. By inducing key metabolo-structural changes on the surface of the bacteria, itaconate modifies the immunostimulatory properties of *P. aeruginosa*, resulting in host-adapted variants that evoke an itaconate-driven immune response permissive, and even supportive, of chronic infection. These findings indicate that host immunometabolism must be considered in future translational therapies addressing multidrug resistant pneumonia.

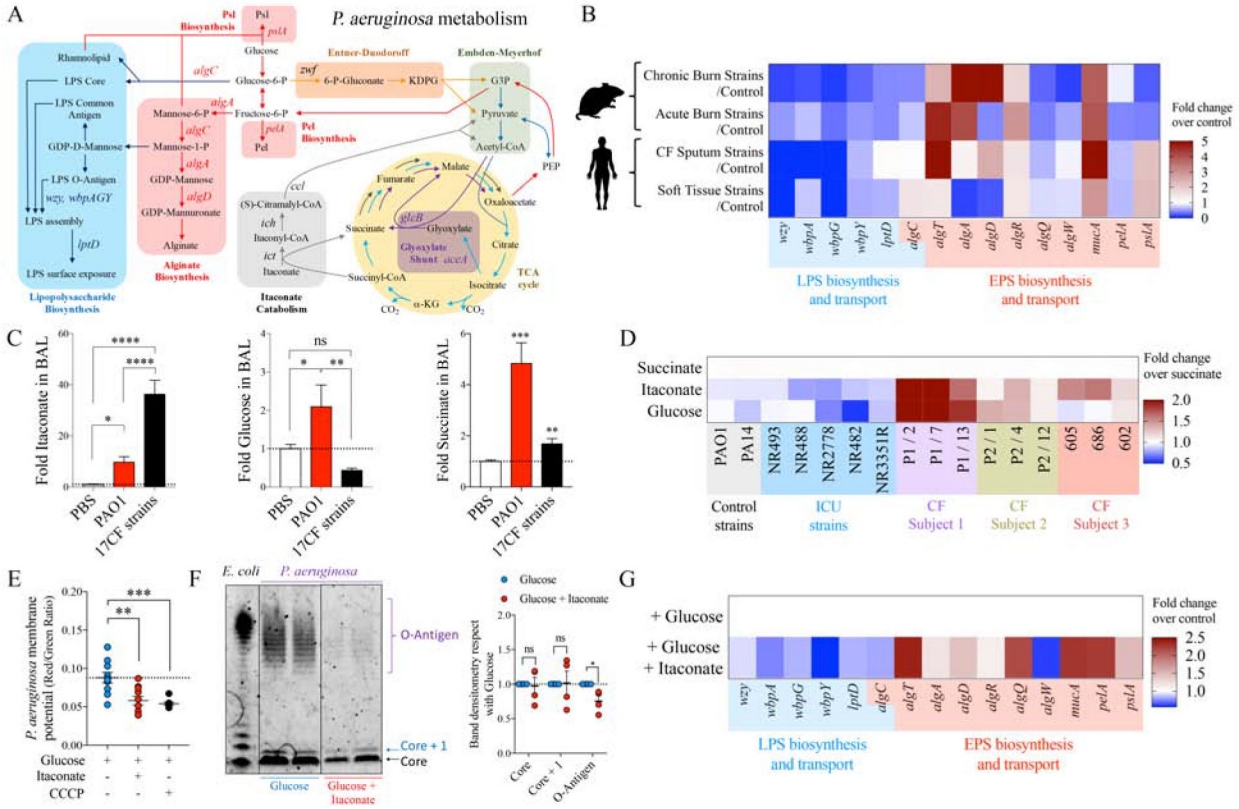

Figure 1.

Metabolic preferences of *P. aeruginosa* in the airway.

A) Scheme showing how metabolism regulates extracellular polysaccharides (EPS) (red box) and lipopolysaccharide (LPS) (blue box) synthesis and transport in *P. aeruginosa*. Itaconate metabolism (gray box), TCA cycle activity (yellow circle) and glucose catabolism (orange-green boxes) are also shown. Gluconeogenic flux is shown as red arrows.

B) Compared with their respective controls (fold increase), expression of different genes involved in EPS and LPS production by *P. aeru*ginosa isolates from mouse and human subjects.

C) Airway abundance of succinate, itaconate and glucose by Mass-Spec in mice infected with *P. aeruginosa* PAO1 or a collection of 17 CF host-adapted *P. aeruginosa* isolates. PBS-treated mice are controls. 4–5 mice pooled from n=2 independent experiments.

D) Fold overnight growth of each *P. aeruginosa* strain with respect to succinate: laboratory strains, ICU and CF isolates are from different subjects.

E) *P. aeruginosa* membrane potential as measured by flow cytometry with *bac*light $DiOC_2(3)$ dye after overnight glucose incubation with or without itaconate (1:1). Membrane potential uncoupler CCCP was used for 30min as positive control for dye specificity.

F) LPS extracts from PAO1 grown overnight in glucose or glucose and itaconate (1:1) and stained for O-antigen and core. *E.coli* LPS: positive control. Respect to glucose only, core, core + 1 and O-antigen LPS band intensities for PAO1 grown in glucose and itaconate were quantified with FIJI.

Author Manuscript Author Manuscript Author Manuscript Author Manuscript

Author Manuscript Author Manuscript Author Manuscript Author Manuscript

G) Fold increase of genes involved in EPS and LPS synthesis in PAO1 growth in glucose and itaconate, with respect to growth only in glucose.

C, E: One-Way ANOVA; **F**: Student's *t*-test. Data are shown as average +/− SEM. **D-G** represent at least n = 3. ****: $P < 0.0001$; ***: $P < 0.001$; **: $P < 0.01$; *: $P < 0.05$; ns: non-significant. See also Figure S1.

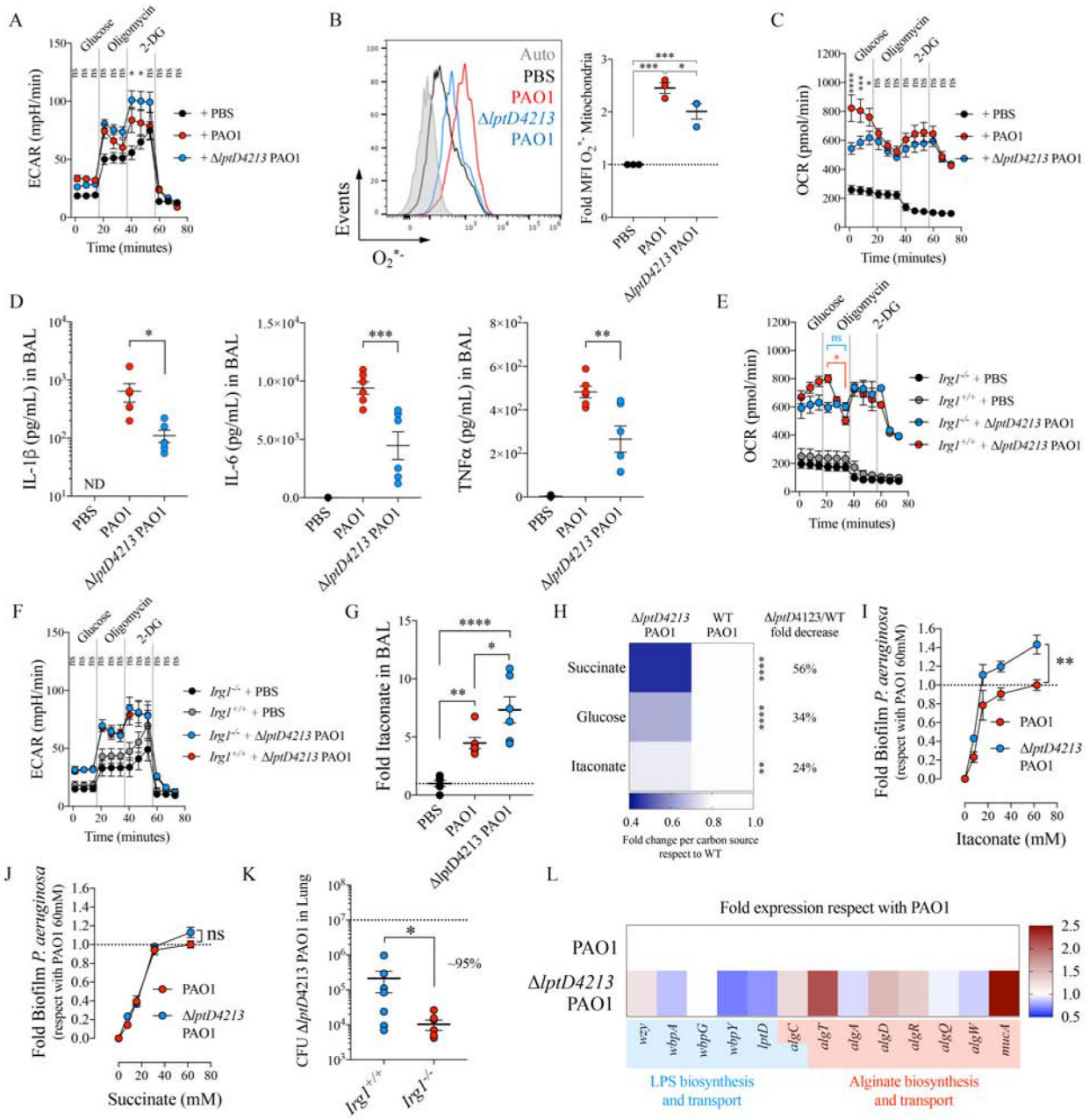

Figure 2.

Δ*lptD*4213 PAO1 induces macrophage itaconate metabolism in the airway.

A-C) Extracellular acidification rates (ECAR) by Seahorse (A), mitochondrial ROS (O_2^{*-}) as determined by Mitosox and flow cytometry (B), and oxygen consumption rates (OCR) by Seahorse (C) in mouse BMDMs either uninfected (PBS) or infected with PAO1 or Δ*lptD*4213 PAO1.

D) Levels of the inflammatory cytokines IL-1β (left), IL-6 (middle) and TNFα (right) in the BAL from uninfected (PBS) or 16h-intranasally infected mice with PAO1 or Δ*lptD*4213 PAO1.

Author Manuscript Author Manuscript Author Manuscript Author Manuscript

Author Manuscript Author Manuscript Author Manuscript Author Manuscript

E-F) The OCR (E) and the ECAR (F) for *Irg1*$^{+/+}$ and *Irg1*$^{-/-}$ BMDMs that were either uninfected (PBS) or infected with Δ*lptD*4213 PAO1.

G) Mice were infected as in D and itaconate was quantified by Mass Spec in BAL.

H) Respect with WT PAO1, Δ*lptD*4213 PAO1 fold overnight growth in different carbon sources.

I-J) Crystal violet biofilms produced by PAO1 and Δ*lptD*4213 PAO1 strains growth in M9 supplemented either with itaconate or succinate.

K) Bacterial burden (CFUs) measured in *Irg1*$^{+/+}$ and *Irg1*$^{-/-}$ lungs of mice infected with Δ*lptD*4213 PAO1.

L) Fold increase of genes involved in EPS and LPS synthesis in Δ*lptD*4213 PAO1, in respect to PAO1. Data are shown as average +/− SEM. **B, D, G**: One-Way ANOVA; **K**: t-Student; **A, C, E-F, I-J**: Two-Ways ANOVA. In vivo data are from n = 2 (6–7 mice total). Seahorse were a minimal of n = 3. ****: $P < 0.0001$; ***: $P < 0.001$; **: $P < 0.01$; *: $P < 0.05$; ns: non-significant. See also Figure S2.

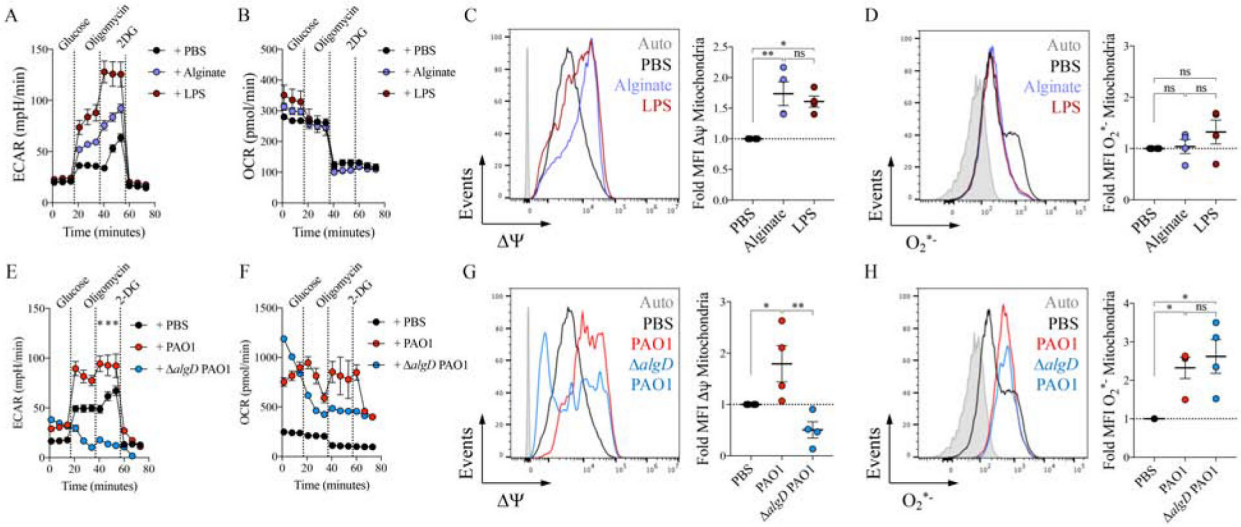

Figure 3.

P. aeruginosa EPS alginate induces anti-oxidant itaconate metabolism.

A-D) Extracellular acidification rate (ECAR) (A) and oxygen consumption rate (OCR) (B) by Seahorse, and mitochondrial membrane potential ΔΨ (C) and mitochondrial ROS ($O_2{*}^-$) (D) by flow cytometry in mouse BMDMs either untreated (PBS) or treated with alginate or LPS.

E-H) The ECAR (E), the OCR (F), the ΔΨ (G), and the $O_2{*}^-$ levels (H) in mouse BMDMs treated with PBS, WT PAO1 or Δ*algD* PAO1.

Data are shown as average +/− SEM. **C-D**, **G-H**: One-Way ANOVA. Seahorse and flow cytometry experiments were a minimal of n=3. ****: $P < 0.0001$; ***: $P < 0.001$; **: $P < 0.01$; *: $P < 0.05$; ns: non-significant. See also Figure S3.

Author Manuscript Author Manuscript Author Manuscript Author Manuscript

Author Manuscript Author Manuscript Author Manuscript Author Manuscript

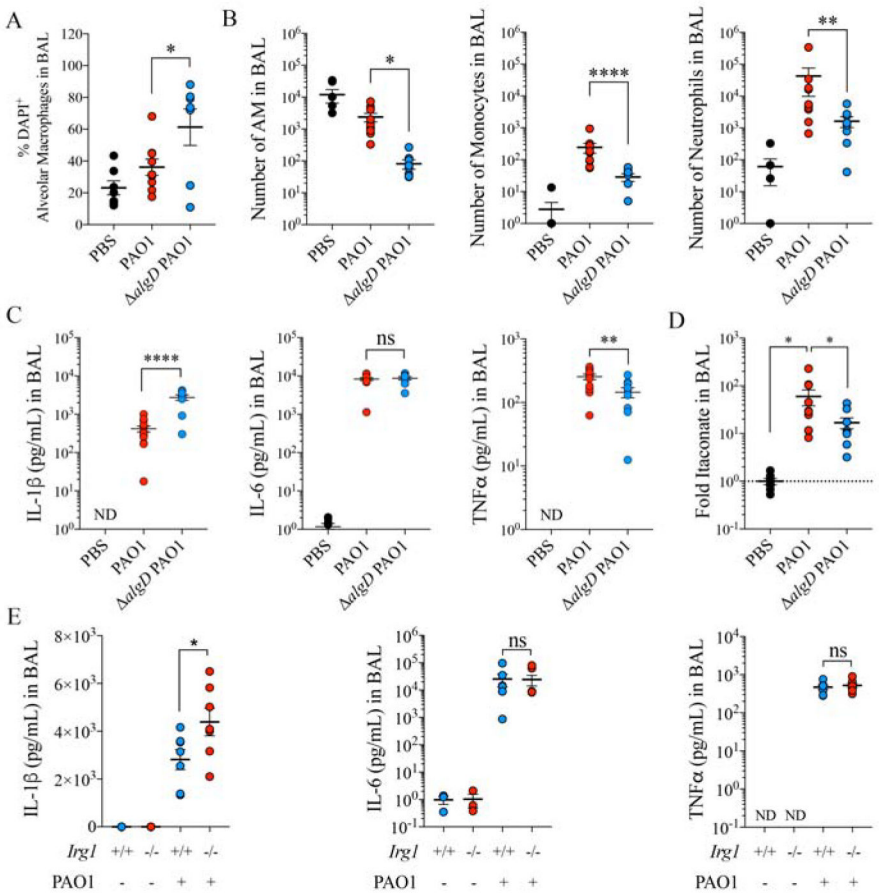

Figure 4.

P. aeruginosa EPS alginate induces airway itaconate and prevents from cell death.

A-D) Percentage of DAPI^{+} alveolar macrophages (death cells) by flow cytometry (A), number of alveolar macrophages (left), Ly6C^{High}Ly6G^{-} monocytes (middle) and neutrophils (right) by flow cytometry (B), pro-inflammatory IL-1β (left), IL-6 (middle) and TNFα (right) cytokines (C) by ELISA and itaconate by Mass Spec (D) in BAL of mice left untreated (PBS) or infected with PAO1 WT or Δ*algD* PAO1.

E) Pro-inflammatory IL-1β (left), IL-6 (middle) and TNFα (right) cytokines in BAL of *Irg1*$^{+/+}$ and *Irg1*$^{-/-}$ mice treated with PBS or infected with PAO1.

Data are shown as average +/− SEM. **A-E**: One-Way ANOVA; Data are from n=2 (7–8 mice total). ****: $P < 0.0001$; ***: $P < 0.001$; **: $P < 0.01$; *: $P < 0.05$; ns: non-significant. See also Figure S3.

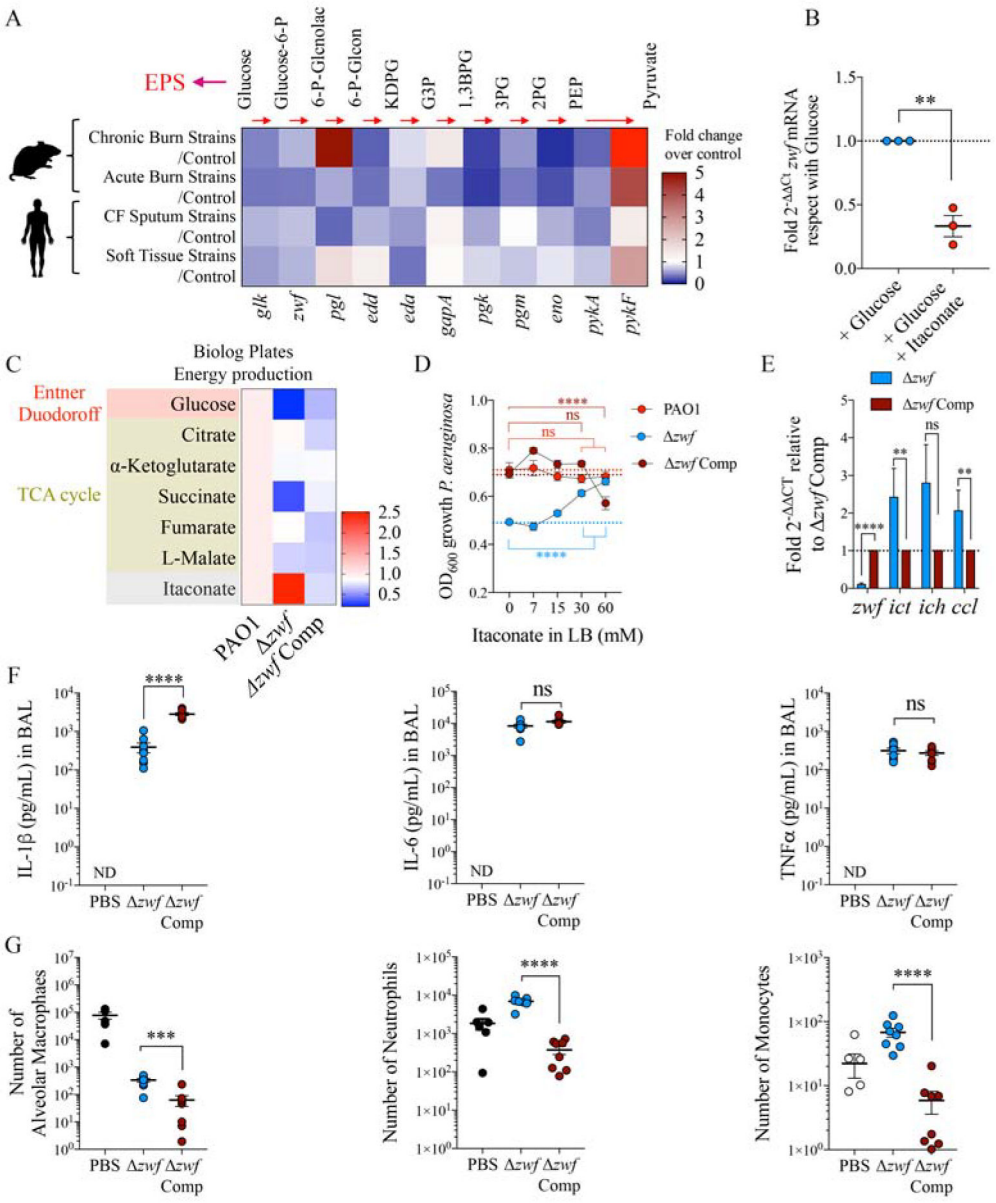

Figure 5.

Reduced glycolytic flux facilitates itaconate assimilation by *P. aeruginosa*.

A) Compared with their respective controls (fold increase), expression of different genes involved in glucose catabolism in *P. aeru*ginosa isolates from mouse and human subjects.

B) *Zwf* mRNA levels by qRT-PCR in M9 + glucose-fed PAO1 exposed or not to itaconate (n=3).

C-E) Energy production by Biolog plates (C), bacterial growth under different itaconate concentrations in LB (D) and *zwf*, *ict*, *ich* and *ccl* mRNA levels by qRT-PCR (E) in Δ*zwf* PAO1 and its complement Δ*zwf* PAO1 Comp control, respect with WT PAO1.

F-G) Pro-inflammatory IL-1β (left), IL-6 (middle) and TNFα (right) cytokines by ELISA (F), and alveolar macrophages (left), Ly6C^{high}Ly6G^{-} monocytes (middle) and

Author Manuscript Author Manuscript Author Manuscript Author Manuscript

Author Manuscript Author Manuscript Author Manuscript Author Manuscript

$Ly6C^{high/low}Ly6G^{+}$ neutrophils (right) numbers by flow cytometry (G) in BAL of mice untreated (PBS) or 16h-infected with Δ*zwf* PAO1 or its Δ*zwf* PAO1 complement control. Data are shown as average +/− SEM. **B, E, F-G**: t-Student. **D**: Two-Way ANOVA. In vivo data are from n=2 (8 mice total). ****: $P < 0.0001$; ***: $P < 0.001$; **: $P < 0.01$; ns: non-significant. See also Figure S4.

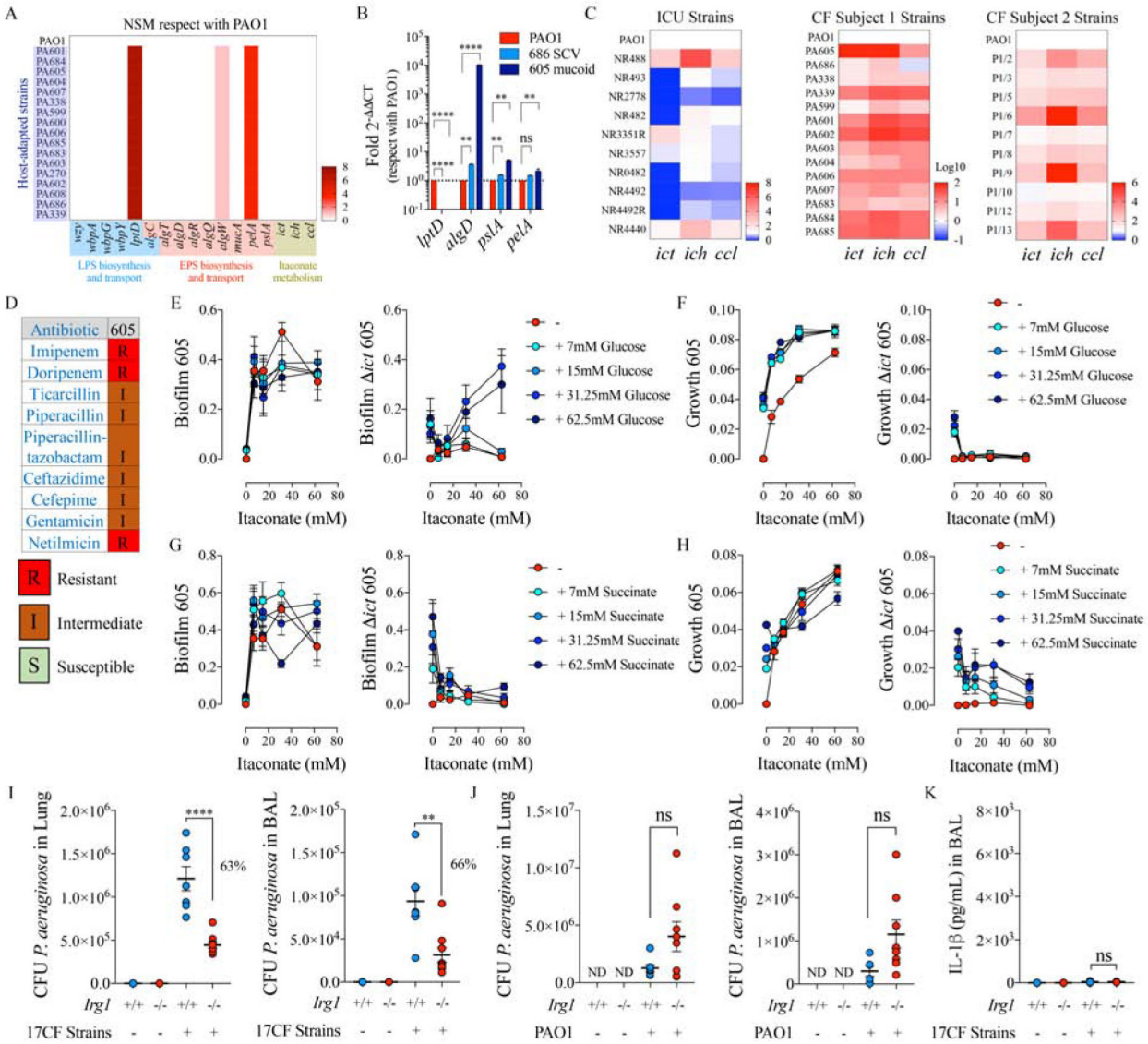

Figure 6.

Host-adapted *P. aeruginosa* isolates exploit host itaconate to colonize the airway.

A) Numbers of non-synonymous SNPs found in a collection of 17 *P. aeruginosa* isolates from an individual with CF, as compared with PAO1 genome. Pathways analyzed: LPS-EPS biosynthesis-trafficking and itaconate catabolism.

B) Fold increase gene expression by qRT-PCR respect with PAO1 in two representative *P. aeruginosa* isolates from A: mucoid 605 and small colony variant 686.

C) *Ict-ich-ccl* locus expression by qRT-PCR in different ICU and CF *P. aeruginosa* isolates, in respect with PAO1.

D) Antibiogram of PA605 mucoid strain.

E-H) Itaconate-mediated both biofilm and growth in presence of glucose (E-F) or succinate (G-H) by mucoid 605 *P. aeruginosa* and its isogenic Δ*ict* mutant.

I-J) Bacterial burden (CFUs) found in *Irg1*$^{+/+}$ and *Irg1*$^{-/-}$ lungs and BALs from mice left untreated (PBS) or infected with CF isolates (I) and PAO1 (J).

Author Manuscript Author Manuscript Author Manuscript Author Manuscript

Author Manuscript Author Manuscript Author Manuscript Author Manuscript

K) IL-1β levels in 17 CF isolates-infected *Irg1*$^{+/+}$ and *Irg1*$^{-/-}$ BALs.

Data are shown as average +/− SEM. **B**: One-Way ANOVA; **I-K**: t-Student. In vivo data are from n=2 (7–8 mice total). ****: $P < 0.0001$; ***: $P < 0.001$; **: $P < 0.01$; *: $P < 0.05$; ns: non-significant. See also Figure S5 and Figure S6.

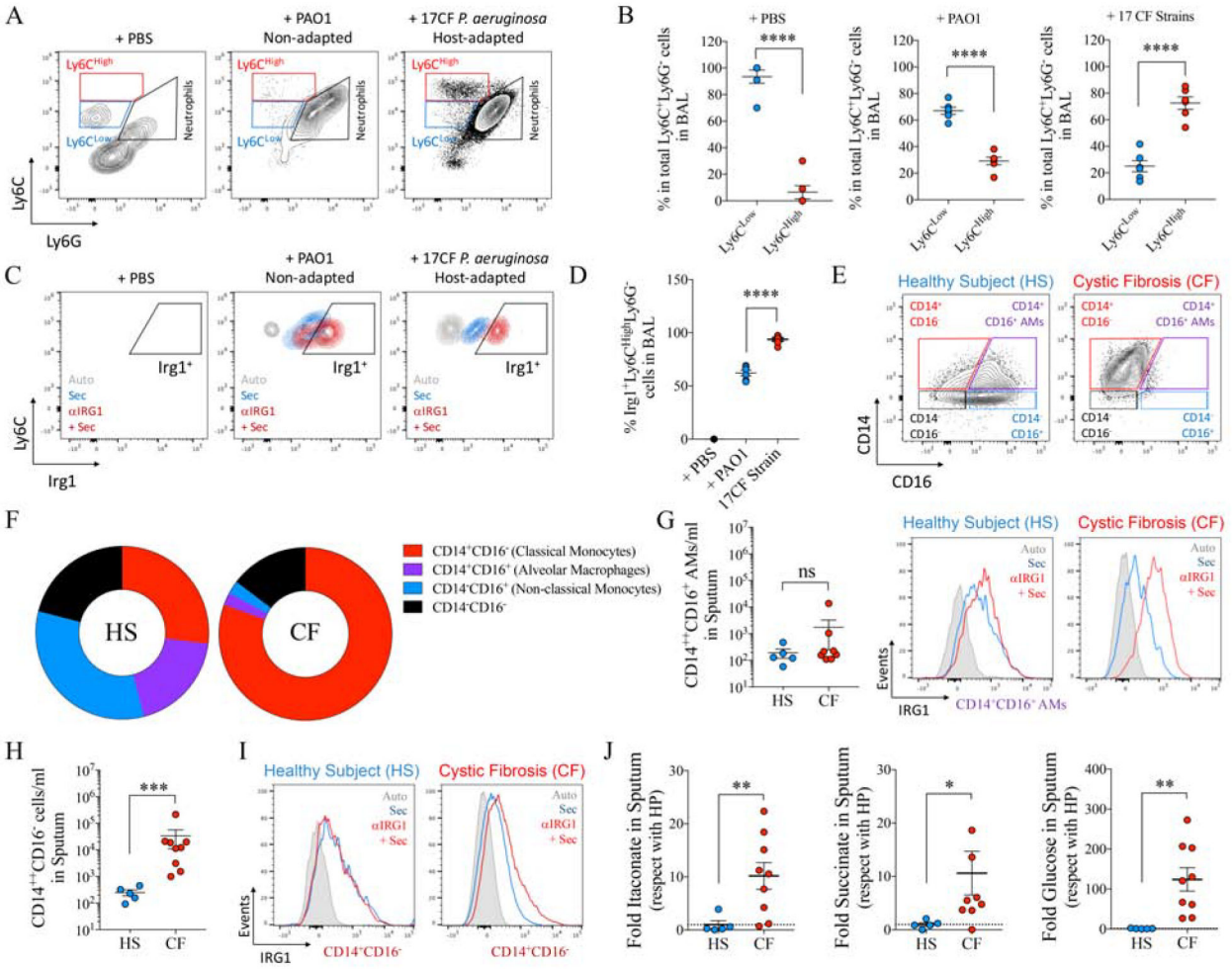

Figure 7.

IRG1 producing airway myeloid cells feed *P. aeruginosa* isolates infection.

A-D) Representative density plots for Ly6C^{high}Ly6G^{-} and Ly6C^{low}Ly6G^{-} monocyte populations (A), their respective percentage in the total Ly6C^{+}Ly6G^{-} population (B) and the percentage of Irg1^{+}Ly6C^{high}Ly6G^{-} population (C-D) in BAL of mice treated with PBS, PAO1 or a collection of 17 CF *P. aeruginosa* isolates.

E-F) Representative density plots (E) and frequency of cells (F) expressing CD14 and/or CD16 surface markers in sputum from healthy subjects (HS) and individuals with CF by flow cytometry.

G) Number of alveolar macrophages (CD14^{+}CD16^{+} in E) found in sputum and their IRG1 expression.

H-I) Number of CD14^{+}CD16^{-} monocytes (shown in E) found in sputum and their IRG1 expression.

J) Sputum metabolomics from healthy subjects (HS) and individuals with CF.

Data are shown as average +/− SEM. **B**, **D**, **G, H, I**: t-Student. In vivo data are from n=2 (5 mice total). In **G, H** and **J** each point represents a single patient. ****: $P < 0.0001$; ***: $P < 0.001$; *: $P < 0.05$; ns: non-significant. See also Figure S7.

Author Manuscript Author Manuscript Author Manuscript Author Manuscript

Author Manuscript Author Manuscript Author Manuscript Author Manuscript

● KEY RESOURCES TABLE

REAGENT or RESOURCE	SOURCE	IDENTIFIER
Antibodies		
Anti-mouse CD45 AF700	Biolegend	Cat 103128, RRID:AB_493715
Anti-mouse CD11c Bv605	Biolegend	Cat 117333, RRID:AB_11204262
Anti-mouse SiglecF	Biolegend	Cat 562680, RRID:AB_2687570
Anti-mouse CD11b AF594	Biolegend	Cat 101254, RRID:AB_2563231
Anti-mouse MHC II APC/Cy7	Biolegend	Cat 107628, RRID:AB_2069377
Anti-mouse Ly6C Bv421	Biolegend	Cat 128032, RRID:AB_2562178
Anti-mouse Ly6G PerCP/Cy5.5	Biolegend	Cat 127616, RRID:AB_1877271
Anti-mouse CD193 FITC	Biolegend	Cat 144509, RRID:AB_2561608
Anti-mouse IRG1	Abcam	ab22241
Anti-mouse IRG1	Abcam	ab222411
Donkey anti-rabbit AF647 IgG H+L secondary antibody	Thermofisher	Cat A31573, RRID:AB_2536183
Anti-human CD45 APC/Fire 750	Biolegend	Cat 304061, RRID:AB_2629700
Anti-human CD19 FITC	Biolegend	Cat 392508, RRID:AB_2750099
Anti-human CD15 BV421	Biolegend	Cat 323040, RRID:AB_2566520
Anti-human CD3 PercP-Cy5.5	Biolegend	Cat 317336, RRID:AB_2561628
Anti-human CD14 AF700	Biolegend	Cat 301822, RRID:AB_493747
Anti-human CD16 PE/Cy7	Biolegend	Cat 302016, RRID:AB_314216
Anti-human CD11b BV605	Biolegend	Cat 301332, RRID:AB_2562021
Anti LPS O_5 antigen	MediMabs	MM-76605-100
Anti LPS A-band	MediMabs	MM-0264
Biological Samples		
Blood PBMCs	This Study	N/A
CF sputum samples	This Study	N/A
Chemicals, peptides and Recombinant Proteins		
Itaconic acid	Sigma Aldrich	I29204
Succinic acid	Sigma Aldrich	14160
α-D-Glucose	Sigma Aldrich	G8270
Sodium alginate	Sigma Aldrich	W201502
Polyethylene glycol 200	Sigma Aldrich	8.07483
Polyethylene glycol 8000	Sigma Aldrich	1546605
Polyethylene glycol 20000	Sigma Aldrich	8.18897
N-acetyl glucosamine	Sigma Aldrich	A8625
Trizol™ Reagent	Thermofisher	15596026
Novex™ 10–20% Tricine Protein Gels	Thermofisher	EC6625BOX
Pro-Q™ Emerald 300 Lipopolysaccharide Gel Stain Kit	Thermofisher	P20495
Live/Dead DAPi dye	Thermofisher	Cat L34962

Author Manuscript Author Manuscript Author Manuscript Author Manuscript

REAGENT or RESOURCE	SOURCE	IDENTIFIER
MitoProbe DilC1 (5)	Thermofisher	Cat M34151
Mitosox	Thermofisher	Cat M36008
*Bac*Light™ Bacterial Membrane Potential Kit	Thermofisher	B34950
Critical Commercial Assays		
Mouse Cytokine Array / Chemokine Array 31-Plex	Evetechnologies	MD31
Seahorse XFe24 FluxPaks	Agilent Technologies	102340-100
RNeasy Mini Kit	Qiagen	Cat 74104
E.Z.N.A.® Total RNA Kit I	Omega Biotek	R6834-01
DNA free removal kit	Thermofisher	AM1906
High-Capacity cDNA Reverse Transcription Kit	Applied Biosystems	4368813
Power SYBR™ Green PCR Master Mix	Applied Biosystems	4368577
Experimental Models: Organisms/Strains		
Mouse: C57BL/6	Jackson Laboratories	JAX: 000664
Mouse: C57BL/6J/N	Jackson Laboratories	JAX: 005304
Mouse: C57BL/6 *Irg1*$^{-/-}$ (*Acod1*$^{-/-}$)	Jackson Laboratories	JAX: 029340
Bacterial and Virus Strains		
P. aeruginosa WT PAO1	Our laboratory	N/A
P. aeruginosa Δ*ict* PAO1	This study	N/A
P. aeruginosa isolate 605 control	This study	N/A
P. aeruginosa isolate Δ*ict* 605	This study	N/A
P. aeruginosa WT PAO1	Provided by Dr. J. Goldberg; Limoli et al, 2017	N/A
P. aeruginosa Δ*algD* PAO1	Provided by Dr. J. Goldberg; Limoli et al, 2017	N/A
P. aeruginosa WT PAO1	Provided by Dr. CJ Balibar; Balibar et al, 2015	N/A
P. aeruginosa Δ*lptD*4213 PAO1	Provided by Dr. CJ Balibar; Balibar et al, 2015	N/A
P. aeruginosa Δ*zwf* PAO1	Provided by Dr. D.E. Ohman; Silu-Suh et al, 2005	N/A
P. aeruginosa Δ*zwf* PAO1 Complemented (Carb^{R})	Provided by Dr. D.E. Ohman; Silu-Suh et al, 2005	N/A
CF subject 3 CF *P. aeruginosaa* isolates	Riquelme et al, 2019	N/A
CF subject 1 *P. aeruginosa* isolates	Provided by Dr. Barbara Kahl	N/A
CF Subject 2 CF *P. aeruginosa* isolates	Provided by Dr. Barbara Kahl	N/A
ICU *P. aeruginosa* isolates	Provided by Dr. A.C. Uhlemman	N/A
Oligonucleotides		
zwf - qzwf-F: GAAGGTATCTCCCTGCAAGT	Riquelme et al, 2019	N/A
zwf - qzwf-R: GGTAGGTCTCGGAAAAACTC	Riquelme et al, 2019	N/A
ict - qict-F: CCTACAGCAGCATCCTTT	This study	N/A
ict - qict-R: CTGGTAGGCGTAGTACATC	This study	N/A
ich - qich-F: AGCACGACATCGTCTACC	This study	N/A

Author Manuscript Author Manuscript Author Manuscript Author Manuscript

REAGENT or RESOURCE	SOURCE	IDENTIFIER
ich - qich-R: ACATAGGGCCAGTCGTAGT	This study	N/A
ccl - qccl-F: AACAGATTCTCGGTCACG	This study	N/A
ccl - qccl-R: GATGGATGCACAGCAAC	This study	N/A
Recombinant DNA		
Yeast strain InvSc1	Thermofisher	C81000
UQ950 *E. coli* DH5 λ*pir* train for cloning	Provided by Dr. Lars Dietrich	N/A
BW29427 *E. coli* donor strain for conjugation	Provided by Dr. Lars Dietrich	N/A
pMQ30 7.5Kb mobilizable vector *oriT*, *sacB*, Gm^R	Provided by Dr. Lars Dietrich	N/A
Software and Algorithms		
GraphPad Prism 8.3.1	GraphPad Software	www.graphpad.com
FlowJo X Flow cytometry	FlowJo	https://www.flowjo.com
FIJI	FIJI	http://imagej.net
Deposited data		
P. aeruginosa RNAseq from mice tissue	Turner et al, 2014 (doi: 10.1371/journal.pgen.1004518)	Accession Number SRP033652
P. aeruginosa RNAseq from humans and mice tissue	Conforth et al, 2018 (doi: 10.1073/pnas.1717525115)	Accession Number SRP135669
Other		
RPMI 1640 1x with glutamine	Corning	10-040-CV
Antibiotic Penicillin-Streptomycin	Corning	30-002-CI
Fetal Bovine Serum	Gibco	26140-079
Biolog plates PM1 and PM2A	Biolog	12111
Irradiated Purina regular chow mice diet	Purina	5053